Fluctuating hydrodynamic interfaces: Theory and simulation

Eirik G. Flekkøy* and Daniel H. Rothman
Department of Earth, Atmospheric, and Planetary Sciences,
Massachusetts Institute of Technology, Cambridge, Massachusetts 02139
(Received 4 May 1995; revised manuscript received 2 November 1995)

The hydrodynamics and statistical mechanics of fluctuating fluid interfaces, both in and out of equilibrium, are studied theoretically and by computer simulation. Theoretically, we show how uncorrelated stresses in the fluids give rise to a correlated force on the interface, i.e., how a Markovian hydrodynamic description with many degrees of freedom reduces to a non-Markovian description of the interface with fewer degrees of freedom. As a key part of this description, we obtain a fluctuation-dissipation theorem that relates the correlations in this thermal force to the hydrodynamic response function of the interface. Simulations are performed with a two-dimensional momentum-conserving lattice-gas model. Results show that an initially flat interface roughens in a manner that satisfies dynamical scaling. Specifically, the time-dependent root-mean-square width $W(L,t)$ of an interface with an initial length L grows like $L^{1/2}f(t/L^{3/2})$, where f is a scaling function such that $W(t) \sim t^{1/3}$ at early times and $W(L) \sim L^{1/2}$ at late times. Except for a logarithmic correction in the static behavior of large-L simulations, both scaling laws are found to to be in good agreement with predictions based on the fluctuation-dissipation theorem. Also, as an independent validation of the simulation method, the equilibrium power spectrum of the interface height is computed and found to be well described by the theory.

PACS number(s): 47.11.+j, 05.40.+j, 68.10.−m

I. INTRODUCTION

In two immiscible fluids, molecular motion excites capillary waves on the interface over a wide range of length and time scales. These waves may be probed experimentally by nonintrusive techniques such as light scattering [1,2]. Theoretical and experimental work, some of it quite recent [3,4], suggests that such thermally excited capillary waves may be important for understanding the physics of droplet breakup [5,6].

On length and time scales between those pertaining to molecular motions and those associated with continuum hydrodynamics, the effect of thermal fluctuations in fluids is well described by the addition of a fluctuating stress tensor to the equations of incompressible hydrodynamics [7]. This stress tensor, which is assumed to be uncorrelated in space and time, gives rise to a corresponding uncorrelated motion in the bulk of the fluid. However, in the presence of moving boundaries, the motion caused by the hydrodynamic coupling between the motion in the bulk and the motion of the boundaries causes space and time correlations to arise. These correlations may be described in terms of hydrodynamic functions that give the response of the system to an external force. In other words, the fluctuations may be related to the dissipation in the system by a *fluctuation-dissipation theorem.*

Such a fluctuation-dissipation theorem was derived by Hauge and Martin-Löf [8] for the case in which the boundary was that of a Brownian particle. Correlations in the force acting on the particle from the fluid were derived. From this result, Hauge and Martin-Löf were able to predict the long-lived correlations in the velocities of Brownian particles, the so-called *long-time tails* that had been previously observed in molecular-dynamics simulations by Alder and Wainwright [9].

Here the same formalism based on fluctuating hydrodynamics is used to obtain a similar fluctuation-dissipation theorem in the case where the boundary is the interface between two immiscible fluids [10]. It is shown that the decay of the resulting correlation function is exponential rather than algebraic, as in the case of the Brownian particle. This correlation function follows from the frequency power spectrum which characterizes the equilibrium state of the interface.

A key component of our study is the comparison of our theoretical predictions with results from numerical simulations of fluctuating interfaces in two-dimensional fluids. (The numerical method—lattice gas cellular automata—is itself interesting, as we point out later in this Introduction.) We focus our attention on two particular aspects of fluctuating interfaces. First, both to verify our theory and to validate our numerical method, we compare computations of the equilibrium frequency power spectrum of interface heights to theoretical predictions. Second, we examine the nonequilibrium roughening (i.e., growth) of an initially flat interface that decays to its equilibrium state. This second aspect of the problem does not appear to have been previously studied. One of our principal results is that the roughening of the interface satisfies a dynamical scaling law.

Interface growth and roughening is the first of two

*Present address: Ecole Supérieure de Physique et Chimie Industrielle, PMMH, 10 rue Vauquelin, 75005 Paris, France.

main points of interest in our study. Recently, numerous models for the nonequilibrium growth of interfaces have been proposed and studied [11–13]. These models range from discrete-particle models for deposition on a substrate to continuum models given in terms of partial differential equations, such as the Edwards-Wilkinson [14] and Kardar-Parisi-Zhang (KPZ) [15] equations. Such studies have typically been concerned with purely local growth, with the only relevant field being the interface itself. In contrast, we study explicitly the coupling between interface growth and a fluctuating hydrodynamic field. Thus the underlying dynamics that governs growth in our case is qualitatively different from the aggregation processes usually studied in the kinetic roughening of growing interfaces [11–13]. Fluctuating fluid interfaces therefore present a challenging link between hydrodynamics and the conceptual framework developed in previous studies of interface growth.

To be more specific, we note that, in our case, the fluctuation-dissipation theorem, which gives the time correlations of the force from the interface on the fluid, can also be used to obtain the roughening of an interface which is initially flat. This is a nonequilibrium process (although not far from equilibrium) which is analogous to the process of relaxation from the ballistic to the diffusive phase of a Brownian particle. However, whereas the root-mean-square displacement of a Brownian particle increases linearly with time t in the ballistic phase, the root-mean-square width W of the interface, which derives from a sum of different Fourier modes growing at different speeds, has, in general, a nonlinear time dependence in the roughening phase. Due to surface tension, $W(t)$ does not increase indefinitely, as in the case of the position of a diffusing particle, but instead reaches an asymptotic value. The two-dimensional case ($d = 2$) for a system of linear size L is characterized by the dynamical (or finite-size) scaling law

$$W(L,t) = L^{\chi} f\left(\frac{t}{L^z}\right) , \tag{1}$$

where f is a scaling function such that $W \sim t^{\chi/z}$ for early times and $W \sim L^{\chi}$ for late times, with $\chi = 1/2$ and $z = 3/2$. The higher dimensional cases, however, are more complicated. In these cases W depends on a second length scale, the shortest wavelength a available to the system. For this reason, $W(t)$ is not given by a simple power law in t when $d > 2$. For large t, W depends logarithmically on L in three dimensions and becomes L independent in higher dimensions. These scaling laws can be obtained from the general framework of the fluctuation-dissipation theorem. But they can also be derived by a simple phenomenological argument that relies on a picture of the interface motion as a sum of standing capillary waves that are distributed in energy according to the equipartition theorem.

Equation (1) is not a new description of interface roughening. Statistical solutions to both the Edwards-Wilkinson [14,16] and KPZ [15] equations satisfy it; moreover, various particle aggregation models show the same average evolution [11,13,17]. In addition, however, we have found such scaling for interface growth coupled to a hydrodynamic field, a richer (albeit more complicated) problem. There is yet one additional curiosity. Surprisingly, and presumably by coincidence, the values of the exponents in the hydrodynamic problem match those which may be derived from the KPZ equation in two dimensions. In both cases, the main point of interest is the so-called *dynamic exponent* z; the result $z = 3/2$ implies a kind of "superdiffusive" roughening. In the KPZ case, such a result relies crucially on the nonlinearity of the differential equation. Our hydrodynamic theory, however, is completely linear.

The second point of interest in our study is the method we use to simulate interfaces. Because we are studying hydrodynamic phenomena whose time and length scales span the gap between microscopic molecular dynamics and macroscopic continuum mechanics, we need a method that can efficiently incorporate a wide range of scales. Rather than simulating the full molecular dynamics, we use lattice-gas cellular automata [18,19], which may be viewed as a kind of discretized (and therefore more efficient) molecular dynamics. Specifically, a two-dimensional fluid is modeled as a collection of identical discrete particles that hop from site to site on a hexagonal lattice and obey simple collision rules that conserve mass and momentum. To simulate interfaces, we use a variant of the original lattice gas known as the *immiscible lattice gas* [20], one of a growing collection of discrete-velocity models of immiscible fluids [21]. Importantly, the discrete nature of lattice gases provides a natural noise source for microscopic fluctuations, which in turn give rise to fluctuating hydrodynamics at a macroscopic scale.

Because the lattice gas method is constructed from a highly idealized microdynamics, the precise relation of its macroscopic behavior to real hydrodynamics has been an active area of research [19,22–24]. Both the average dynamics and some important aspects of the fluctuation dynamics of lattice gases are now relatively well understood. Dynamical effects of the intrinsic fluctuations in lattice gases have been studied in the case of pure fluids [24,25] and for fluids with suspended, Brownian particles [26,27].

Lattice-gas models of interfaces (immiscible fluids) are, however, less well understood [21]. Broadly speaking, this relative lack of understanding stems from the unusually severe simplifications made in the immiscible fluid models. The most important of these simplifications is the lack of detailed balance, i.e., the microdynamics is irreversible. It is therefore of great interest to quantify the extent to which immiscible lattice gases capture the physics of real fluid interfaces. For this purpose, we compare our lattice-gas simulations with a theory which is classical in the sense that it relies on the usual physical assumptions of detailed balance and the possibility of defining a temperature. We find that both the equilibrium state (i.e., the frequency power spectrum of heights) and the nonequilibrium behavior (i.e., the roughening) of our idealized fluid interfaces are well described by the incompressible (fluctuation-dissipation) theory up to a sharply defined upper frequency, above which the compressibility and density fluctuations of the lattice gas be-

come important. Previous studies of interfaces in immiscible lattice gases have concentrated on the prediction of surface tension [28,29] and nonhydrodynamic aspects of interface fluctuations [29]. The present study is a detailed investigation of *moving* interfaces in immiscible lattice gases and how they couple dynamically to microscopic fluctuations. Given the ostensibly inadequate microphysics and the lack of thermodynamics in immiscible lattice gases, the good agreement that we find between simulations and classical fluctuating hydrodynamics is remarkable.

The paper is organized as follows. First the general framework of fluctuating hydrodynamics is reviewed and the boundary conditions that couple the interface to the fluctuating fluid are defined. Following this, the fluctuation-dissipation theorem is derived from a Green's identity that is obtained from the unsteady Stokes equations in a separate Appendix. The fluctuation-dissipation theorem contains a hydrodynamic response function $\gamma_{\mathbf{k}}(t)$ which gives the interface response to an external force. For the sake of completeness and readability, the relevant solution of the unsteady Stokes equations is derived. A general equation of motion describing the response of an interface with surface tension to an arbitrary forcing is derived in terms of the interface degrees of freedom only. On the basis of this equation and the correlations of the thermal force the power spectrum for the interface heights is derived in the general case of a d-dimensional system. In order to quantify the importance of the correlations in the thermal force, the power spectrum corresponding to an uncorrelated force is derived and compared to the spectrum of a correlated force. Following this, the theoretical predictions for the roughening and scaling behavior of the interface are obtained from the low viscosity limit of the fluctuation-dissipation theory. Finally, we provide a short review of the immiscible lattice gas and compare the results of simulations to the theoretical predictions for the frequency power spectrum of interface heights and the time-dependent interface growth.

II. THE FLUCTUATING HYDRODYNAMIC DESCRIPTION

In the following we write down the basic equations of fluctuating hydrodynamics and define the interface in mathematical terms through the boundary condition on the fluctuating part of the velocity field and the stress tensor. In order to complete the fluctuating hydrodynamic description, the fluctuating stress tensor s_{ij} must be included. We review briefly how the statistical properties of s_{ij} may be derived from nonequilibrium statistical mechanics. This amounts to deriving the fluctuation-dissipation relation on the level of the uncorrelated forces in the bulk of the fluids. From this result we derive the fluctuation-dissipation theorem on the level of the correlated force on the interface. Following this, the response function $\gamma_{\mathbf{k}}(t)$, which is needed as input to the fluctuation-dissipation theorem, is obtained.

By this development the resulting description of the interface, which is contracted from the full Markovian description of the fluid (with more degrees of freedom), reduces to a non-Markovian description in two ways. In addition to the non-Markovian character intrinsic to the time correlations of the fluctuating force, the response function relates the interface height function to the entire history of the (external or internal) force on the interface. The fluctuation-dissipation theorem states that these two, apparently different, forms of history dependence have the same origin.

A. The equations of motion and the boundary conditions

The description of a fluctuating incompressible fluid is given by the Navier-Stokes equations [7]

$$\partial_t \mathbf{u} + \mathbf{u} \cdot \nabla \mathbf{u} = -\frac{\nabla P}{\rho} + \nu \Delta \mathbf{u} + \mathbf{f}, \tag{2}$$

$$\nabla \cdot \mathbf{u} = 0, \tag{3}$$

where $\mathbf{u}$ and P are the velocity and pressure, ν the kinematic viscosity of the fluid, ρ the mass density, ∂_t and Δ denote the time derivative and ∇^2, respectively, and equations can be taken to have an arbitrary dimension d. The fluctuating force per unit volume represents the thermal motion in the fluid. On time scales much larger than the molecular mean free time the temporal correlations in $\mathbf{f}$ can be neglected. Throughout the paper we shall limit the discussion to the case where the two fluids have equal viscosities and densitites.

For a given wavelength λ the $\mathbf{u}\cdot\nabla\mathbf{u}$ term is of the order $\omega^2 A_\lambda^2/\lambda$, where A_λ is the amplitude and ω the frequency of the oscillations. The $\partial_t \mathbf{u}$ term is of the order $A_\lambda \omega^2$. Hence, for an oscillating fluid the $\mathbf{u} \cdot \nabla \mathbf{u}$ term is smaller than the $\partial_t \mathbf{u}$ term by a factor A_λ/λ. The assumption of small amplitudes seems to be consistent with both the theoretical and the simulated results, and in the following we will work with the linearized equations.

Equations (2) and (3) with the nonlinear term removed constitute the Markovian starting point for our analysis. In the next section we examine the fluctuating force. The fluctuating force in Eq. (2) causes the velocity and pressure fields to split into a slowly varying part and a fluctuating part that vanish upon averaging. So we write

$$\begin{aligned} \mathbf{u} &= \overline{\mathbf{u}} + \tilde{\mathbf{u}}, \\ P &= \overline{P} + \tilde{P}, \end{aligned} \tag{4}$$

where $\overline{\mathbf{u}}, \overline{P}$ and $\tilde{\mathbf{u}}, \tilde{P}$ denote the averaged and fluctuating parts, respectively. By averaging the linearized version of Eqs. (2) and (3) we obtain the nonfluctuating equations

$$\partial_t \overline{\mathbf{u}} = -\frac{\nabla \overline{P}}{\rho} + \nu \Delta \overline{\mathbf{u}}, \tag{5}$$

$$\nabla \cdot \overline{\mathbf{u}} = 0 \tag{6}$$

and the corresponding equations

$$\partial_t \tilde{\mathbf{u}} = -\frac{\nabla \tilde{P}}{\rho} + \nu \Delta \tilde{\mathbf{u}} + \mathbf{f}, \tag{7}$$

$$\nabla \cdot \tilde{\mathbf{u}} = 0 \tag{8}$$

for the fluctuating part of the fields. The two sets of equations above appear decoupled. However, as will be seen below, the fluctuating fields couple to the nonfluctuating ones through the boundary condition on the interface.

The vertical force per area $\mathbf{F}_A(\mathbf{x},t)$ on the interface I from the fluid A (see Fig. 1) is given by

$$\mathbf{F}_A(\mathbf{x},t) = -\mathbf{n} \cdot \boldsymbol{\sigma} \tag{9}$$

and the force from the fluid $(A+B)$

$$\mathbf{F}(\mathbf{x},t) = -\mathbf{n} \cdot [\boldsymbol{\sigma}(B) - \boldsymbol{\sigma}(A)] \tag{10}$$

$$\equiv -\mathbf{n} \cdot [\boldsymbol{\sigma}] \,, \tag{11}$$

where the stress tensors in the first line of the above equation are evaluated at $z = 0$ on the B and A sides of the interface, respectively. The vector $\mathbf{n}$ is the unit normal vector to the interface, pointing in the positive z direction. The stress tensor is defined as

$$\boldsymbol{\sigma} = -\mathbf{I}\, P + \rho\nu \left(\nabla \mathbf{u} + \nabla \mathbf{u}^T\right) \tag{12}$$

where $\mathbf{I}$ is the identity tensor and T denotes the transpose. We shall employ the linearizing approximation that the stress tensor on the right hand side of Eq. (9) is evaluated at $z = 0$, and not at the exact position of the interface. Since $\boldsymbol{\sigma}$ is a linear function of the pressure and the velocity it follows that the force $\mathbf{F}_A$ also decomposes into a fluctuating and an average part:

$$\mathbf{F}_A(\mathbf{x},t) = \overline{\mathbf{F}}_A(\mathbf{x},t) + \tilde{\mathbf{F}}_A(\mathbf{x},t) \tag{13}$$

where

$$\overline{\mathbf{F}}_A(\mathbf{x},t) = \mathbf{n} \cdot \boldsymbol{\sigma}(\overline{\mathbf{u}}, \overline{P}),$$

$$\tilde{\mathbf{F}}_A(\mathbf{x},t) = \mathbf{n} \cdot \boldsymbol{\sigma}(\tilde{\mathbf{u}}, \tilde{P}) \,. \tag{14}$$

If the interface were a passive tracer surface without surface tension or mass, it would simply follow the fluid and the boundary condition would be that the velocity of the interface be that of the fluid. However, when there is surface tension there will be a discontinuity in the stress tensor across the interface, and the interface will act on the fluid with a force that will partially suppress the fluctuating fluid motion. The reason for this is that due to the hydrodynamics a volume of linear size k^{-1} must be moved in order to excite a perturbation of wave number $\mathbf{k}$ on the interface. Hence, inertial forces as well as the surface tension will counteract deformations of the interface. We shall make the approximation that on the interface the fluctuating part of the velocity vanishes entirely, i.e., that

$$\tilde{\mathbf{u}}(\mathbf{x},t) = \mathbf{0} \text{ when } \mathbf{x} \in I \,. \tag{15}$$

Neglecting nonlinear terms again, the corresponding boundary condition on the interface height is

$$\overline{u_z}(\mathbf{x},t) = \dot{h}(\mathbf{x},t) \text{ when } \mathbf{x} \in I \,. \tag{16}$$

Hence the interface motion will be given entirely in terms of $\overline{F}$. The above boundary condition is illustrated in Fig. 2, which gives a qualitative picture of the velocity on the interface and in the bulk. The velocity shown is Fourier transformed in coordinates parallel to the interface. In the bulk the velocity has a rapidly fluctuating component $\tilde{\mathbf{u}}$ that vanishes upon ensemble averaging leaving a systematic slowly varying part. On the interface $\tilde{\mathbf{u}}$ is shown to vanish.

To a first approximation the statistical average employed is over different realizations of the fluctuating fields in the bulk of the fluid consistent with a *given* motion of the interface. However, as we shall see, the interface motion is itself driven by $\tilde{F}$. Hence, the velocity on the interface will receive a small fluctuating component due to the feedback mechanism between the interface and the fluid. This fluctuating component can in principle be put back in Eq. (15) to correct the boundary condition. However, we shall assume that such an iterative scheme would converge sufficiently rapidly that Eq. (15) already gives an adequate description of the interface.

The theory to follow will largely be formulated in Fourier space, and for later reference we define the proper transforms now as

$$h_{\mathbf{k}}(t) = \frac{1}{A} \int dS\, e^{-i\mathbf{k}\cdot\mathbf{x}} h(\mathbf{x},t) \tag{17}$$

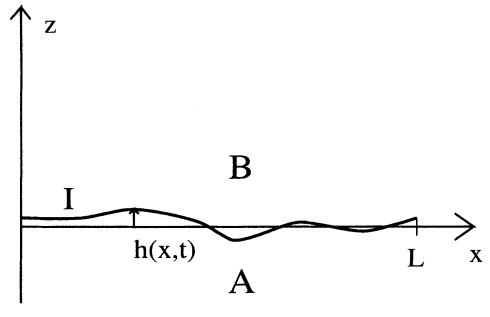

FIG. 1. The height of the interface as a function of x and t. The interface separates the two parts of the fluid $\mathcal{A}$ and $\mathcal{B}$. L is the system length. In three dimensions the surface $A = L^2$.

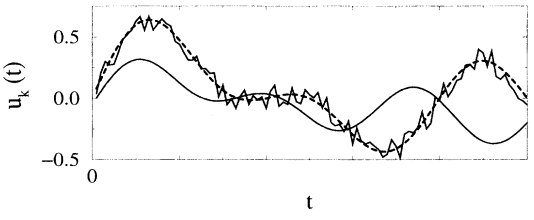

FIG. 2. The (z component of the) velocity measured on I (smooth full line) and in the bulk (noisy full line). The dashed line shows $\overline{u}_{z\mathbf{k}}$.

with the inverse

$$h(\mathbf{x},t) = \sum_{\mathbf{k}} e^{i\mathbf{k}\cdot\mathbf{x}} h_{\mathbf{k}}(t), \tag{18}$$

where in two dimensions $\mathbf{k}$ has only one component $k_x = 2\pi n/L$ and $n = 0, \pm 1, \pm 2, ...$, and in d dimensions $\mathbf{k} = (2\pi/A)\mathbf{n}$ and $\mathbf{n}$ is a vector with integer components. A is the area of the flat interface; in two dimensions $A = L$, and the integration $\int dS$ becomes $\int_0^L dx$. We will denote the spatial Fourier transform by the same symbol with a subscript for the wave number, whereas we will assign a caret to quantities which are also transformed in the time domain. Thus

$$\hat{h}_{\mathbf{k}}(\omega) = \frac{1}{2\pi} \int dt\, h_{\mathbf{k}}(t) e^{-i\omega t}, \tag{19}$$

$$h_{\mathbf{k}}(t) = \int d\omega\, \hat{h}_{\mathbf{k}}(\omega) e^{i\omega t}\,. \tag{20}$$

B. The fluctuating hydrodynamic force

The behavior of the fluctuating force $\mathbf{f}$ in Eqs. (2) and (3) is obtained from statistical mechanics [7,8]. Hauge and Martin-Löf [8] do this by analogy with the finite-dimensional Gaussian Markov process. Hinch does it on the basis of a generalized Langevin equation and the equipartition principle [30]. We shall, for the sake of completeness, briefly review the conceptual structure of the derivation of Hauge and Martin-Löf and the connection between their result and the standard result for the fluctuating part of the stress tensor [7]. Being uncorrelated in time the autocorrelation function can be written

$$\langle f_i(\mathbf{x},t) f_j(\mathbf{x}',t')\rangle = U_{ij}(\mathbf{x}-\mathbf{x}')\delta(t-t') \tag{21}$$

where $U_{ij}(\mathbf{x}-\mathbf{x}')$ is some unknown amplitude function depending on the spatial separation, and $\mathbf{f}$ is real. Viewing the linearized version of Eq. (2) as a Langevin equation for the pair $(\mathbf{u}, P)$, the mean square fluctuation of $(\mathbf{u}, P)$ can be written down in terms of U. However, it is known that the probability of a fluctuation $(\mathbf{u}, P)$ is given by the corresponding increase of the entropy $\Delta\mathcal{S}$ from the equilibrium value of $(\mathbf{u}, P)$ through

$$e^{(-\Delta\mathcal{S}/k_B)}\,, \tag{22}$$

where k_B and T are the Boltzmann constant and the temperature, respectively. The above Boltzmann factor relates the amplitudes U_{ij} and $\Delta\mathcal{S}$, which, when Taylor expanded around the equilibrium values of $(\mathbf{u}, P)$, is a quadratic function in $(\mathbf{u}, P)$. By the hypothesis that the averaged decay of a microscopic fluctuation of $(\mathbf{u}, P)$ is given by the noiseless (unsteady) Stokes equations, U can be related to the entropy production $d\Delta\mathcal{S}/dt$ instead of the entropy itself. This relation has the form [8]

$$2T\frac{d\Delta\mathcal{S}}{dt}\delta(t-t') = \frac{1}{k_B T}\int dV dV'\ \langle \mathbf{u}(\mathbf{x},t)\cdot\mathbf{f}(\mathbf{x},t)\,\mathbf{f}(\mathbf{x}',t')\cdot\mathbf{u}(\mathbf{x}',t')\rangle \tag{23}$$

where the domain of integration is the entire space occupied by the fluid. Since the entropy production (times T) is simply the heat generated by the viscous dissipation [7]

$$T\frac{d\Delta\mathcal{S}}{dt} = D(\mathbf{u}) \equiv \rho\nu \int dV\ \left(\partial_j u_i\, \partial_j u_i + \partial_j u_i\, \partial_i u_j\right), \tag{24}$$

we get the relation

$$2k_B T D(\mathbf{u})\delta(t-t') = \int dV\, dV' \langle \rho\mathbf{u}(\mathbf{x},t)\cdot\mathbf{f}(\mathbf{x},t)\,\mathbf{f}(\mathbf{x}',t')\cdot\rho\mathbf{u}(\mathbf{x}',t')\rangle\,. \tag{25}$$

This equation is the fluctuation-dissipation theorem on the level of the Markovian force $\mathbf{f}$. In the next section we shall use this result to obtain the fluctuation-dissipation relation for the integrated force $\tilde{F}$.

The fluctuating force is often written as the divergence of a fluctuating part of the stress tensor

$$\mathbf{f} = \nabla\cdot\mathbf{s}\,. \tag{26}$$

The stress s_{ij} gives the forces due to the thermal motion in the fluid, and it should be considered as the driving force for all the subsequent motion. In contrast to s_{ij}, the stress $\tilde{\sigma}$ represents the fluctuating part of the entire stress in the fluid, which includes the pressure and the viscous forces. Inserting the above expression for $\mathbf{f}$ in Eq. (25) and performing a partial integration, comparison with Eq. (24) shows that a possible choice for the autocorrelation function of s_{ij} is given as

$$\langle s_{ik}(\mathbf{x},t)s_{jl}(\mathbf{x}',t')\rangle = 2k_B T\rho\nu\delta(\mathbf{x}-\mathbf{x}')\delta(t-t') \times [\delta_{ij}\delta_{kl} + \delta_{il}\delta_{kj}] \text{ when } \mathbf{x}\notin I, \tag{27}$$

$$\boldsymbol{s}(\mathbf{x},t) = \mathbf{0} \text{ when } \mathbf{x}\in I\,. \tag{28}$$

Equation (27) is the standard basis [7] for the fluctuating hydrodynamics of an incompressible fluid.

Hauge and Martin-Löf [8] discuss the possible boundary conditions for the force on the interface, and they show that it is possible to allow $\boldsymbol{s}$ to have the same values on the interface as in the bulk. In this case a corresponding force $-\mathbf{n}\cdot[\mathbf{s}]$ would have to be added to the equation of motion for the interface in order to ensure momentum conservation. The equation of motion for the interface will be introduced in the following. However, both conservation of momentum and the fluctuation-dissipation theorem for $\mathbf{f}$ are satisfied with the choice of Eqs. (27) and (28). For the sake of mathematical simplicity we will stay with the description of Eqs. (27) and (28) and the form of $\tilde{F}$ given in Eqs. (13) and (14) as the only fluctuating force acting on the interface.

III. THE HYDRODYNAMIC RESPONSE

In this section we obtain the hydrodynamic response function of a fluid subject to an external vertical forc-

ing. This result will be needed in the next section where we show that the fluctuation-dissipation theorem simply gives the correlations of the force on the interface in terms of this response function.

We shall consider a single, but arbitrary, Fourier component of the interface force, given by $\mathbf{k}$ and ω. In the three-dimensional case we shall align the x axis with $\mathbf{k}$, thus effectively reducing the problem to two dimensions. The form of the response function will be independent of dimension. Indeed, in the following, dependence on the number of dimensions will only enter when contributions from different wave numbers $\mathbf{k}$ are summed.

The fluid and the interface will be considered as two separate systems — one acting on the other with a force. It is assumed that this force will produce low amplitude oscillations of the fluid, and hence that the unsteady Stokes equations will give an appropriate description of the fluid. Then, due to the linearity of the problem, the general response to an external force is readily obtained by superposing different Fourier modes.

A. The solution of the unsteady Stokes equation

The mathematical form of the problem given by Eqs. (5) and (6) describing the velocity field $\mathbf{u}$, and the boundary condition on the force on the interface as given by Eq. (11), takes the form

$$\begin{aligned} F(x,t) &= -[n_i\sigma_{iz}] \\ &\approx -[\sigma_{zz}] \\ &= F_0 e^{i(\mathbf{k}\cdot\mathbf{x}-\omega t)} , \end{aligned} \tag{29}$$

where F_0 is the amplitude of the force per unit area acting from the fluid on the interface — or, by Newton's third law, the force acting from the interface on the fluid. This force will later be identified with the surface tension and the fluctuating forces acting at the position of the moving interface in a direction normal to it. We will require continuity of the velocity

$$[\mathbf{u}] = \mathbf{0}, \tag{30}$$

where the square brackets denote the change in $\mathbf{u}$ across the boundary, and we will impose the condition

$$[\sigma_{xz}] = 0 , \tag{31}$$

where the stress tensor is defined in Eq. (12). This condition means that there can be no force from the interface on the fluid acting in the direction along the interface. This would correspond to a spatially varying surface tension. These boundary conditions along with Eqs. (5) and (6) fully determine the flow field.

We will decompose the velocity field as

$$\mathbf{u} = \mathbf{u}_\nu + \mathbf{u}_P \tag{32}$$

where $\mathbf{u}_P$ satisfies the linearized Euler equation

$$\partial_t \mathbf{u}_P = -\frac{\nabla P}{\rho} \tag{33}$$

and $\mathbf{u}_\nu$ satisfies the diffusion equation

$$\partial_t \mathbf{u}_\nu = \nu \Delta \mathbf{u}_\nu . \tag{34}$$

We note that $\mathbf{u}_P$ couples to the pressure, but is independent of the viscosity, while $\mathbf{u}_\nu$ is independent of the pressure, but depends on the viscosity. In the present case of oscillating flow, mass conservation must be satisfied independently by the two components of the velocity field, i.e.,

$$\nabla \cdot \mathbf{u}_\nu = \nabla \cdot \mathbf{u}_P = 0 . \tag{35}$$

This results from the following. Taking the divergence of Eq. (5) gives $\nabla^2 P = 0$ and consequently $\partial_t \nabla \cdot \mathbf{u}_P = 0$. It follows that $\nabla \cdot \mathbf{u}_P$ must be time independent. But since the flow is oscillating this can only happen if $\nabla \cdot \mathbf{u}_P = 0$. By Eq. (6) it then follows that also $\nabla \cdot \mathbf{u}_\nu = 0$.

By taking the curl on both sides of Eq. (33) we obtain

$$\partial_t \nabla \times \mathbf{u}_P = \mathbf{0} \tag{36}$$

from which it follows that $\nabla \times \mathbf{u}_P = \text{const} = \mathbf{0}$, since the flow oscillates. In two dimensions the curl of the velocity field will be understood to be the scalar $\partial_z u_x - \partial_x u_z$. Consequently there exists a velocity potential such that

$$\mathbf{u}_P = \nabla \Phi. \tag{37}$$

It follows from the Euler equation and the assumption that $\mathbf{u} = \mathbf{0}$ at $t = -\infty$ that

$$P = -\rho \partial_t \Phi. \tag{38}$$

The condition of mass conservation on $\mathbf{u}_P$ then takes the form

$$\Delta \Phi = 0 \tag{39}$$

which implies that

$$\Delta \mathbf{u}_P = \mathbf{0}. \tag{40}$$

This result shows that $\mathbf{u}$ given by Eqs. (32)–(34) is indeed a solution of the unsteady Stokes equation. In view of the boundary conditions we will seek solutions of the form

$$\mathbf{u}_\nu(x,z,t) = \mathbf{w}(z) e^{i(\mathbf{k}\cdot\mathbf{x}-\omega t)}, \tag{41}$$

$$\Phi(x,z,t) = \Phi_0(z) e^{i(\mathbf{k}\cdot\mathbf{x}-\omega t)}. \tag{42}$$

The diffusion equation and the Euler equation then take the form

$$\begin{aligned} \partial_z^2 \Phi_0 - k^2 \Phi_0 &= 0, \\ \partial_z^2 \mathbf{w} + \left(\frac{i\omega}{\nu} - k^2 \right) \mathbf{w} &= \mathbf{0} , \end{aligned} \tag{43}$$

where $k = |\mathbf{k}|$. Due to the equality of the fluids below and above the interface, P and hence Φ must be odd functions of z. Also, u_x and u_z must be odd and even functions of z, respectively. By requiring that the flow velocity be finite at $z = \pm\infty$, the solutions of the above equations can be written

$$\Phi_0(z) = -v_0 \frac{\mathrm{sgn}(z)}{k} e^{-k|z|}, \tag{44}$$

$$\mathbf{w}(z) = w_0 \left[-q \frac{k_x}{k^2} \mathrm{sgn}(z),\ 1\right] e^{iq|z|}, \tag{45}$$

where sgn denotes the sign, the vector given in the brackets is chosen so that $\nabla \cdot \mathbf{u}_\nu = 0$, and

$$q = k\sqrt{\frac{i\,\omega}{k^2\nu} - 1}\,. \tag{46}$$

The square root in the above expression is defined by a branch cut along the negative imaginary axis, so that the argument of the square root will not pass the branch cut for any ω or k, and q will always have a positive imaginary part.

The velocity field obtained from Eq. (45) is

$$u_x = -\left(i\,v_0 e^{-|kz|} + w_0 \frac{q}{k} e^{-i\,q|z|}\right) \mathrm{sgn}(z)\, e^{i(\mathbf{k}\cdot\mathbf{x}-\omega t)},$$
$$u_z = \left(w_0 e^{i\,q|z|} + v_0 e^{-k|z|}\right) e^{i(\mathbf{k}\cdot\mathbf{x}-\omega t)}. \tag{47}$$

Since u_x is an odd function of z, the continuity condition implies that

$$u_x(x, 0, t) = 0. \tag{48}$$

This gives one of the conditions on the integration constants. The other condition is obtained from Eq. (29) by substituting the velocity field of Eq. (47) and the pressure from Eq. (38) in Eq. (12). This gives

$$\sigma_{zz} = -\frac{q\omega\rho}{k^2} w_0\, \mathrm{sgn}(z) e^{i(\mathbf{k}\cdot\mathbf{x}-\omega t)}. \tag{49}$$

It is easily shown that σ_{xz} (and σ_{yz} and σ_{xy} in three dimensions) is automatically continuous across the interface when Eq. (48) is satisfied. Substituting Eq. (49) in Eq. (29) gives v_0 and w_0 in terms of the external force, and we obtain the final form of the velocity field:

$$u_x = \frac{k_x F_0}{2\omega\rho}\left(e^{-k|z|} - e^{i\,q|z|}\right) \mathrm{sgn}(z)\, e^{i(\mathbf{k}\cdot\mathbf{x}-\omega t)},$$
$$u_z = \frac{kF_0}{2\omega\rho}\left(i\,e^{-k|z|} + \frac{k}{q} e^{i\,q|z|}\right) e^{i(\mathbf{k}\cdot\mathbf{x}-\omega t)}. \tag{50}$$

The applied forcing on the interface is given in the form of a moving wave. For the sake of visualizing the velocity field, we construct the corresponding standing wave by adding the two fields given by $\mathbf{k}$ and $-\mathbf{k}$. The two-dimensional streamlines for (the real part of) this velocity field are shown in Fig. 3 for some different times. The closed vortex forms right after the interface velocity has changed sign and exists only for a short time τ_1. In fact, an infinite cascade of vortices exists. We label them sequentially with a number $i = 1, 2, 3, \ldots$ increasing away from the interface. Their lifetime τ_i decreases exponentially with i. As the flow field itself is exponentially damped with i, the higher order vortices ($i > 1$) are vanishingly weak. A similar cascade of vortices ex ists in the low Reynolds number flow past a sharp corner of sufficiently small opening angle. They were described theoretically by Moffatt in 1964 [31]. They differ from the vortices in the present case by their time independence, and by the fact that not only their strength, but also their spatial size decays exponentially with i. The present vortices resemble the vortices which are shed from an oscillating sphere or ellipsoid [32] by their time dependence. However, it appears that an infinite *cascade* of time-dependent vortices has not been previously observed.

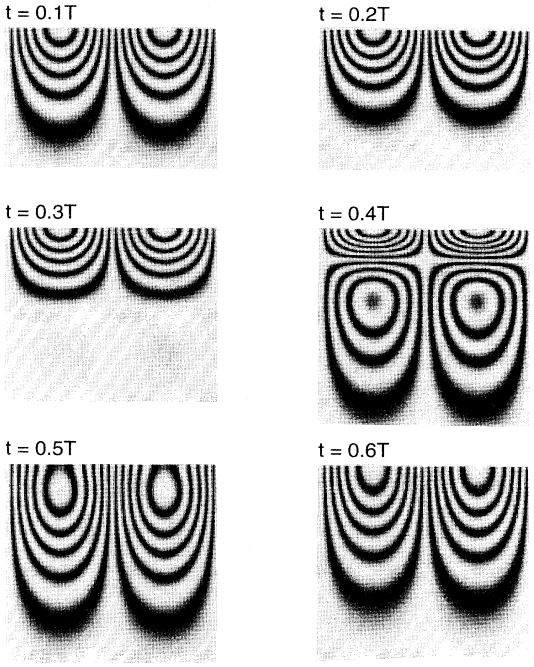

FIG. 3. The streamlines shown at various instants of time t. The thicker streamlines correspond to a smaller velocity. T is the period of the oscillations. The ratio of the viscous time to the period (times 2π) is $\alpha = \omega/(k^2\nu) = 1$. The horizontal base of each figure is one wavelength $2\pi/k$.

B. The response function

If the interface is forced to move with a prescribed velocity $\dot{h}(x,t)$, the fluid will respond by setting up velocity and pressure fields given by Eqs. (5) and (6). This field will act back on the interface in a way specified by the stress tensor. Since both Eqs. (5) and (6) and the stress tensor are linear in the velocity and pressure field it follows that the force on the interface itself must be given by $\dot{h}(x,t)$ in a linear form. This remains true also when the relevant quantities are Fourier transformed. The linearity ensures that different Fourier modes are uncoupled. The most general relation between the interface height and the applied force is then of the form

$$\overline{F}_{\mathbf{k}}(t) = \frac{1}{2\pi}\int_{-\infty}^{\infty} dt'\, \gamma_{\mathbf{k}}(t-t')\, \dot{h}_{\mathbf{k}}(t')\,, \tag{51}$$

where the interface velocity is $\dot{h}_{\mathbf{k}}$, $\overline{F}_{\mathbf{k}}$ is the average force, and the response function is $\gamma_{\mathbf{k}}$. Equation (51) is the

non-Markovian relation between the force applied on the interface and its motion. Note that it could have been written in the opposite, and perhaps more intuitive, way, giving the motion of the interface in response to the force. However, we are free to interpret either quantity as the dependent one. The motion of the interface is dependent not only on the instantaneous value of the force, but, in general, on all previous values, or, in the other picture, the force needed to maintain a prescribed motion depends in general on the entire history of the motion.

The right hand side of Eq. (51) is a convolution of $\gamma_{\mathbf{k}}$ and $\dot{h}_{\mathbf{k}}$, which upon Fourier transforming in time becomes a simple product:

$$\hat{F}_{\mathbf{k}}(\omega) = \hat{\gamma}_{\mathbf{k}}(\omega)\ \hat{\dot{h}}_{\mathbf{k}}(\omega)\ . \tag{52}$$

But $\hat{F}_{\mathbf{k}}(\omega)$ can simply be taken as F_0 in Eq. (29). The interface velocity $\dot{h}_{\mathbf{k}}$ is given in Eq. (16).

It is now a simple matter to read off the response function from Eq. (50). It can be written

$$\hat{\gamma_{\mathbf{k}}}(\omega) = \frac{2\omega\rho}{k(i+\frac{k}{q})}\ . \tag{53}$$

As a result of causality $\gamma_{\mathbf{k}}(t) = 0$ for negative t. This follows from the unsteady Stokes equation from which $\gamma_{\mathbf{k}}(t)$ is derived. It can be seen by Fourier transforming the above expression, using the definition Eq. (19), and noting that for negative t the Fourier integral giving $\gamma_{\mathbf{k}}(t)$ can be evaluated by integration along a contour in the upper complex ω plane. In this half plane $\hat{\gamma_{\mathbf{k}}}(\omega)$ has no poles, and the integral vanishes. Hence the integral in Eq. (51) only samples past values of $\dot{h}_{\mathbf{k}}$. Equation (53) is the result we need to evaluate the autocorrelation of the fluctuating part of the force on the interface.

IV. THE FLUCTUATION-DISSIPATION THEOREM AND THE FORCE AUTOCORRELATION FUNCTION

In this section we derive the fluctuation-dissipation theorem. It relates the correlations in the fluctuating force $\tilde{F}$ on the interface to the (dissipative) hydrodynamic response to an external forcing, given by the response function $\gamma_{\mathbf{k}}(t)$, which will be obtained in the next section. The starting point for the derivation of the theorem will be a Green's identity which is derived in Appendix A. The Green's identity is based solely on the equations of motion for the fluctuating and average velocity and pressure fields and the equations giving their boundary conditions on the interface. Hence it contains no other physical information than that contained in these equations. It reads as follows. If $\overline{\mathbf{u}}$ and $\overline{P}$ satisfy Eqs. (5) and (6) and $\tilde{\mathbf{u}}$ and $\tilde{P}$ satisfy Eqs. (7) and (8) and the boundary conditions are given by Eqs. (15) and (16) for any *given* $\dot{h}(\mathbf{x},t)$, then

$$0 = \int_{-T}^{T} dt \int d\mathbf{S}\cdot\tilde{\boldsymbol{\sigma}}(\mathbf{x},t)\cdot\ \overline{\mathbf{u}}(\mathbf{x},-t) + \int_{-T}^{T} dt \int_{\mathcal{A}} dV\ \overline{\mathbf{u}}(\mathbf{x},-t)\cdot\mathbf{f}(\mathbf{x},t) \tag{54}$$

where T is some large time which will eventually be taken to infinity, $d\mathbf{S}$ points away from the fluid $\mathcal{A}$, $\tilde{\boldsymbol{\sigma}}$ is defined by the fluctuating velocity and pressure, and all quantities are real. Here the integration is taken only over the lower part of the fluid, denoted by the subscript $\mathcal{A}$. The above identity is based on the unsteady Stokes equations (5) and (6) and Eqs. (7) and (8) and the assumption that the driving force vanishes at large negative and positive times, i.e., that $\mathbf{f} = \mathbf{0}$, when $|t| > T$. It also depends on the boundary condition that $\tilde{\mathbf{u}} = \mathbf{0}$ on the interface.

Writing the equation corresponding to Eq. (54) for fluid $\mathcal{B}$ and adding Eq. (54) for fluid $\mathcal{A}$, we immediately obtain

$$0 = \int_{-T}^{T} dt \int d\mathbf{S}\cdot\ [\tilde{\boldsymbol{\sigma}}(\mathbf{x},t)]\cdot\overline{\mathbf{u}}(\mathbf{x},-t) + \int_{-T}^{T} dt \int dV\ \overline{\mathbf{u}}(\mathbf{x},-t)\cdot\mathbf{f}(\mathbf{x},t)\ , \tag{55}$$

where the continuity of $\overline{\mathbf{u}}$ has been used in writing the first term and the volume integration in the last term is over both parts of the fluid.

From the condition that the amplitude of the interface motion be small compared to its wavelength we note that the surface element vector $d\mathbf{S}$ is almost parallel to the z axis, i.e., $dS_k \approx dS\ \delta_{zk}$. Hence we can write $d\mathbf{S}\cdot[\tilde{\boldsymbol{\sigma}}]\cdot\overline{\mathbf{u}}(\mathbf{x},-t) \approx dS\ [\tilde{\sigma}_{iz}]\ \overline{u}_i(\mathbf{x},-t) \approx dS\ [\tilde{\sigma}_{zz}]\ \dot{h}(\mathbf{x},-t) \approx dS\ \tilde{F}(\mathbf{x},t)\ \dot{h}(\mathbf{x},-t)$ where $\tilde{F}$ is the fluctuating force *on* the interface, and in the second line we have assumed that $[\sigma_{iz}] = 0$ when $i \neq z$, i.e., that the off-diagonal terms of the stress tensor be continuous across the interface. This is consistent with the physical requirement of a constant surface tension.

Using the above expressions in Eq. (55) and taking the average of the square of the resulting equation we get

$$\left\langle\left(\int_{-\infty}^{\infty} dt\ \int dS\ \tilde{F}(\mathbf{x},t)\dot{h}(\mathbf{x},-t)\right)^2\right\rangle = \left\langle\left(\int_{-\infty}^{\infty} dt\ \int dV\ \overline{\mathbf{u}}(\mathbf{x},-t)\cdot\mathbf{f}\right)^2\right\rangle = 2k_BT\int_{-\infty}^{\infty} dt\ D(\overline{\mathbf{u}}(\mathbf{x},t)) \tag{56}$$

where Eq. (25) and the substitution $t \to -t$ have been used in the last line. This equation relates the fluctuating force on the interface to the dissipation in the fluid associated with the average velocity $\overline{\mathbf{u}}$. This dissipation can be identified as the work done on the fluid by the average force $\overline{F}$ on the fluid over all of time, i.e.,

$$\int_{-\infty}^{\infty} dt\, D(\overline{\mathbf{u}}) = \int dS \int_{-\infty}^{\infty} dt\, \overline{F}(\mathbf{x},t)\dot{h}(\mathbf{x},t) \tag{57}$$

$$= \int dS \int_{-\infty}^{\infty} dt\, A \sum_{\mathbf{k}} \overline{F}_{\mathbf{k}}(t)\, \dot{h}_{-\mathbf{k}}(t), \tag{58}$$

where we have passed to the Fourier transforms defined in Eqs. (17) and (18).

In Sec. III we derived the linear response of the system to an external forcing. Substituting the expression in Eq. (51) for the force in Eq. (57), Eq. (56) takes the form

$$2\int\int_{t'<t} dt'\, dt\, A^2 \sum_{\mathbf{k}\mathbf{k}'} \dot{h}_{-\mathbf{k}}(t)\, \dot{h}_{\mathbf{k}'}(t') \left\langle \tilde{F}_{\mathbf{k}}(t)\, \tilde{F}_{-\mathbf{k}'}(t') \right\rangle$$

$$= \frac{k_B T A}{\pi} \sum_{\mathbf{k}} \int\int_{t'<t} dt'\, dt\, \dot{h}_{-\mathbf{k}}(t)\gamma_{\mathbf{k}}(t-t')\dot{h}_{\mathbf{k}}(t'), \tag{59}$$

where we have used the substitutions $t \to -t$ and $t' \to -t'$ in the first integral above, and the symmetry $t \leftrightarrow t'$ together with time translational invariance of an equilibrium average to constrain the left hand side integral by $t' < t$. Since Eqs. (54) and (51) hold for an *arbitrary* function $\dot{h}_{\mathbf{k}}(t)$, we can identify the integrands on the left and right hand sides of Eq. (59). This gives

$$\left\langle \tilde{F}_{\mathbf{k}}(t-t')\tilde{F}_{-\mathbf{k}'}(0) \right\rangle = \frac{k_B T}{2\pi A}\, \gamma_{\mathbf{k}}(|t-t'|)\, \delta_{\mathbf{k}\mathbf{k}'} \tag{60}$$

where the time translation invariance of an equilibrium average has again been used. This is the fluctuation-dissipation theorem for the force on the interface written in terms of the **k**th Fourier components of a real force. It links the correlations in the fluctuating force on the interface resulting from the uncorrelated stress fluctuations in the fluid to the hydrodynamic response function γ, which is obtained above from purely continuum mechanical reasoning.

In the following we will need the fluctuation-dissipation relation in terms of the complex force $\tilde{F}_{\mathbf{k}}(t) = \tilde{F}_{1\mathbf{k}}(t) + i\tilde{F}_{2\mathbf{k}}(t)$ where $\tilde{F}_{1\mathbf{k}}(t)$ and $i\tilde{F}_{2\mathbf{k}}(t)$ are the transforms of the real and imaginary parts of $\tilde{F}(\mathbf{x},t)$, respectively. Writing out the fluctuation-dissipation theorem for $\tilde{F}_{1\mathbf{k}}$ and $\tilde{F}_{2\mathbf{k}}$ separately, and using that $\tilde{F}_{1\mathbf{k}}(t)$ and $\tilde{F}_{2\mathbf{k}}(t)$ are uncorrelated and $\tilde{F}^*_{\mathbf{k}}(t) = \tilde{F}_{1-\mathbf{k}}(t) - i\tilde{F}_{2-\mathbf{k}}(t)$, we obtain

$$\left\langle \tilde{F}_{\mathbf{k}}(t)\tilde{F}^*_{\mathbf{k}'}(0) \right\rangle = \frac{k_B T}{\pi A}\, \gamma_{\mathbf{k}}(|t|)\, \delta_{\mathbf{k}\mathbf{k}'}\,. \tag{61}$$

This is the form of the fluctuation-dissipation theorem for a complex force that we will use in the following.

In order to understand the above result it is possible to perform the inverse Fourier transform to get the correlation function explicitly. To Fourier transform the response function in Eq. (61) we introduce a frequency cutoff Ω and write

$$\gamma_{\mathbf{k}}(t) = \int_{-\Omega}^{\Omega} d\omega\, e^{-i\omega t}\hat{\gamma}_{\mathbf{k}}(\omega)\,. \tag{62}$$

Having Ω finite allows interchange of the order of differentiation and integration, and we can write

$$\gamma_{\mathbf{k}}(t) = \frac{\partial}{\partial t}\int_{-\Omega}^{\Omega} d\omega e^{-i\omega t}\frac{\hat{\gamma}_{\mathbf{k}}(\omega)}{-i\omega} \tag{63}$$

where the integrand goes properly to zero for large ω. Hence, we can deform the real axis in the complex ω plane, shown in Fig. 4, and disregard contributions from the C_R contour. By deforming the real axis to C_{cut} (the poles shown by circles are irrelevant here) we get an integral which is easily solved by a simple secondary deformation from the real to the imaginary axis. At this point the exponent of the exponential becomes real instead of imaginary, and the time derivative of the integrand can be carried out. In the $\Omega \to \infty$ limit the result is

$$\left\langle \tilde{F}_{\mathbf{k}}(t)\tilde{F}^*_{\mathbf{k}}(0) \right\rangle = \frac{4\rho k_B T}{Ak}(k^2\nu)^2 \frac{e^{-k^2\nu|t|}}{(k^2\nu|t|)^{3/2}}\,. \tag{64}$$

Hence, the force correlation function is not only divergent but nonintegrable when $t \to 0$. This paradox can be resolved by returning to Eq. (62) where Ω is finite. Integrating Eq. (62) over the time domain $0 < t < T$ and using the asymptotic forms of $\hat{\gamma}_{\mathbf{k}}(\omega)$ it can be observed by interchanging the order of integration that $\int_0^T dt\ \gamma_{\mathbf{k}}(t) \sim \Omega$ when $T > \Omega^{-1}$ and correspondingly that the variance $\langle|\tilde{F}_{\mathbf{k}}|^2\rangle \sim \Omega^2$. Equation (64) is hence valid only for $|t| > \Omega^{-1}$. In a discretized molecular picture of a fluid nothing happens between particle interactions. So if Ω is taken as the rate of particle collisions on a given surface area A, the result that $\langle|\tilde{F}_{\mathbf{k}}|^2\rangle \sim \Omega^2$ simply means that the thermal force results from a sum of collisions between particles of a given thermal velocity. This result is as one would expect from a discrete picture of the fluid, and the divergence of Eq. (64) signals the breakdown of the continuum description given by the hydrodynamic equations and the assumption of a

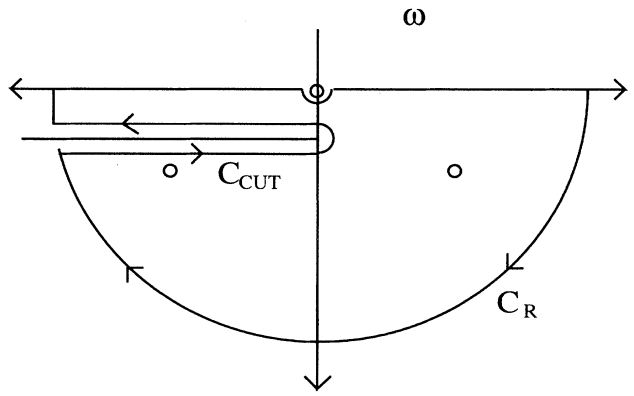

FIG. 4. The integration contour in the complex ω plane. The poles are marked as ○. The poles in the lower half plane give the capillary wave contribution to the height autocorrelation function, whereas the pole at the origin gives a time-independent contribution.

δ-correlated force in Eq. (21). The vanishing correlation time of Eq. (21) corresponds to a vanishing mean free time between collisions and hence to an infinite Ω.

However, the description of the force correlations could be made consistent within a continuum picture as well. By taking the fluid to be compressible and modifying the fluid dynamic equations accordingly, the response function would change, in particular for the high frequencies. Presumably this would remove the divergence of the force correlations since a compressible fluid will have a softer behavior when subjected to very rapid oscillations than will an incompressible fluid.

For later reference we take the $\nu \to 0$ limit of Eq. (64). This is most easily done by taking the limit directly in the response function of Eq. (53). This gives $\hat{\gamma} \to -2i\omega\rho/|k|$ when $\nu \to 0$ and we get

$$\gamma_{\mathbf{k}}(t) = \frac{2\rho}{k}\delta'(t) \tag{65}$$

where $\delta'(t)$ is the derivative of Dirac's delta function. Note that as opposed to the odd $\delta'(t)$ the even function $\delta'(|t|)$ is nonintegrable.

From Eq. (64) it is seen that the region where the force is power-law correlated increases with decreasing viscosity as $(k^2\nu)^{-1}$. The amplitude, on the other hand, decreases with decreasing viscosity as $\sqrt{\nu}$. The point $\nu = 0$ is hence singular in the sense that the force decorrelates completely, whereas for ν slightly larger than zero there is a long-time correlation for $t < (k^2\nu)^{-1}$. For large ν the force decorrelates as $e^{-k^2\nu t}$.

The fact that the inviscid fluid responds without a memory effect, and hence that $\tilde{F}$ becomes uncorrelated, can be understood by considering the solution of the Euler equation given by Eqs. (42) and (44). The streamlines obtained from these equations are time independent, whereas the streamlines obtained from the full unsteady Stokes equation depend on time as shown in Fig. 2. This means that in the Euler case an external sinusoidal force acting on the interface will always move the same amount of fluid in the same way. This in turn means that the acceleration of the fluid in response to the force acting on the interface will everywhere be immediate. We hence conclude that the force correlations stem from the viscous diffusion of momentum. The correlations disappear when the corresponding diffusion time $(k^2\nu)^{-1}$ either vanishes or goes to infinity.

V. THE EQUILIBRIUM STATE

We now turn to the computation of the equilibrium power spectrum and the corresponding interface height autocorrelation function $\langle \dot{h}_{\mathbf{k}}(t)\dot{h}^*_{\mathbf{k}}(0)\rangle$. The long-time behavior of $\langle \dot{h}_{\mathbf{k}}(t)\dot{h}^*_{\mathbf{k}}(0)\rangle$ will be shown to be exponential, rather than algebraic as in the case of Brownian motion [8,9,27].

We shall show that for the height-velocity autocorrelation function $\langle \dot{h}_{\mathbf{k}}(t)\dot{h}^*_{\mathbf{k}}(0)\rangle$ the physical information contained in the fluctuation-dissipation theorem reduces explicitly to the statement that spontaneous fluctuations *on the average* decay as corresponding macroscopic perturbations of the system.

As a starting point we need the equation of motion for $h_{\mathbf{k}}$. This equation is derived in the following, using the picture of the interface and the fluid as two separate, interacting systems as a conceptual guide.

A. Interface equation of motion

Equations (52) and (53) give the response of the interface to an arbitrary external force $\hat{F}$ acting on the fluid. Now, the fluid interface is characterized by a surface tension σ which gives rise to a force per unit area on the fluid which when linearized has the form $\sigma\nabla^2 h$ where the Laplacian is $(d-1)$-dimensional. From Newton's law of action and reaction this force must be equal and opposite to the force F acting from the fluid on the interface. It then follows from Eq. (52) that

$$\hat{\dot{h}}_{\mathbf{k}} = \frac{1}{\hat{\gamma}_{\mathbf{k}}}\hat{\tilde{F}} = -\frac{1}{\hat{\gamma}_{\mathbf{k}}}\left(\sigma k^2 \hat{h}_{\mathbf{k}} + \hat{\tilde{F}}_{\mathbf{k}}\right) . \tag{66}$$

This is the equation of motion for the interface height. Note that since $\dot{h} = \bar{u}_z(I)$ the interface velocity $\hat{\dot{h}}_{\mathbf{k}}$ is written as a response to the *average* force only. The force $\tilde{F}$ cancels the fluctuating part of the surface tension force, which corresponds to the total force on the interface. Hence $\tilde{F}$ acts as the driving force of the motion. Solving Eq. (66) for $\hat{\dot{h}}_{\mathbf{k}}(\omega)$ we get

$$\hat{\dot{h}}_{\mathbf{k}}(\omega) = \Gamma_{\mathbf{k}}(\omega)\,\hat{\tilde{F}}_{\mathbf{k}}(\omega) \tag{67}$$

where we have introduced the second response function

$$\Gamma_{\mathbf{k}}(\omega) = \frac{1}{\hat{\gamma}_{\mathbf{k}}(\omega) - \frac{\sigma k^2}{i\omega}} . \tag{68}$$

If $\hat{\tilde{F}}_{\mathbf{k}}(\omega)$ is taken as an arbitrary force, Eq. (67) is a general description of an interface with surface tension, which is subject to an external or internal force. To investigate the history dependence of this description we take the high and low viscosity limits of Eq. (68),

$$\Gamma_{\mathbf{k}}(\omega) \to \begin{cases} \frac{2k}{\rho i\omega}\frac{1}{1-(\omega_0/\omega)^2}, & k^2\nu \to 0 \\ \frac{1}{4\rho k\nu}\left[1 + O(\frac{1}{k^2\nu})\right], & k^2\nu \to \infty, \end{cases} \tag{69}$$

where

$$\omega_0 = \sqrt{\frac{\sigma}{2\rho}}\,k^{3/2} \tag{70}$$

is the well-known capillary wave dispersion relation for an *inviscid* fluid [7].

The $\nu \to 0$ limit gives a simple propagator for capillary waves, i.e., the equation $(\rho/2k)\dot{h}_{\mathbf{k}}(t) = \int_{-\infty}^{t} dt' F_{\mathbf{k}}(t') e^{-i\omega_0 t'}/(2\omega_0)$, which in physical terms means that the interface motion is a sum of capillary waves excited at previous times. This is a highly non-Markovian description as all previous events are equally weighted. For finite ν the excitations are damped as $e^{-k^2\nu t}$, and there is a characteristic time $(k^2\nu)^{-1}$ over

which the fluid responds with a memory. The high viscosity limit, on the other hand, gives the equation

$$4\rho k\nu \dot{h}_{\mathbf{k}} = \tilde{F}_{\mathbf{k}}, \tag{71}$$

which is like Stokes law and involves no history dependence. Equation (71) can also be viewed as a (Markovian) Langevin equation for a massless object. This corresponds to the fact that the interface has no independent inertial mass. The full description of the interface results when the force in Eq. (67) has the thermal correlations given in Eq. (64). This description is in general non-Markovian on account of both the force correlations and the non-Markovian properties of Eq. (67). In the discussion of the simulations we will return to the issue of the relative importance of these two memory mechanisms.

B. Capillary waves

When there is no other force than the surface tension force, i.e., when $\tilde{F}_{\mathbf{k}} = 0$, Eq. (66) is homogeneous and gives the capillary wave dispersion relation

$$i\omega\hat{\gamma}_{\mathbf{k}}(\omega) - \sigma k^2 = 0 . \tag{72}$$

This relation can be shown to be equivalent to the dispersion relation found in Ref. [33]. In the high viscosity limit this equation gives the imaginary solution

$$\omega = -i\frac{\sigma|k|}{2\rho\nu} \tag{73}$$

to leading order in $1/\nu$. This solution corresponds to an overdamped wave with a characteristic damping time $2\rho\nu/(\sigma|k|)$. This time increases with viscosity and wavelength and decreases with surface tension — as one would expect. In the small-viscosity limit the solutions to lowest order in ν are

$$\omega = \pm\left(\omega_0 - \frac{1}{2}\sqrt{\frac{k^2\nu}{2}\,\omega_0}\right) - \frac{i}{2}\sqrt{\frac{k^2\nu}{2}\omega_0} . \tag{74}$$

It can be shown numerically that, when

$$\frac{k^2\nu}{\omega_0} \leq 1.269 , \tag{75}$$

Eq. (72) has two solutions which are symmetric around the imaginary axis and thus decribe left or right moving capillary waves. When the above inequality does *not* hold, there is only one solution which is purely imaginary, corresponding to waves that are overdamped. Note that, when the inequality holds, the general solution of Eq. (72) $\omega_\pm = \pm\omega_r - i\omega_i$ must have a negative imaginary part in order for the capillary waves to dissipate their energy. Correspondingly, $\Gamma_{\mathbf{k}}(\omega)$ will have no poles in the upper half of the complex ω plane.

C. Height power spectrum

In order to obtain $|\hat{\dot{h}}_{\mathbf{k}}(\omega)|^2$ in terms of the power spectrum of the fluctuating force we take the modulus square of Eq. (67). By Eq. (61) we have

$$|\tilde{F}_{\mathbf{k}}(\omega)|^2 = \frac{\Theta}{(2\pi)^2}\frac{2k_BT}{A}\left[\hat{\gamma}_{\mathbf{k}}(\omega) + \hat{\gamma}_{\mathbf{k}}(-\omega)\right] . \tag{76}$$

Here Θ is the size of the time integration domain. In the end, the $\Theta \to \infty$ limit is implied.

Inserting the above expression for $|\tilde{F}_{\mathbf{k}}(\omega)|^2$ in the square of Eq. (67) and using the expression for $\Gamma_{\mathbf{k}}$, we get

$$|\hat{\dot{h}}_{\mathbf{k}}(\omega)|^2 = \frac{k_BT\,\Theta}{(2\pi)^2 A}\frac{\hat{\gamma}_{\mathbf{k}}(\omega) + \hat{\gamma}_{\mathbf{k}}(-\omega)}{[\hat{\gamma}_{\mathbf{k}}(\omega) - \frac{\sigma k^2}{i\omega}][\hat{\gamma}_{\mathbf{k}}(-\omega) + \frac{\sigma k^2}{i\omega}]} \tag{77}$$

$$= \frac{k_BT\,\Theta}{(2\pi)^2 A}\left(\frac{1}{\hat{\gamma}_{\mathbf{k}}(\omega) - \frac{\sigma k^2}{i\omega}} + \frac{1}{\hat{\gamma}_{\mathbf{k}}(-\omega) - \frac{\sigma k^2}{-i\omega}}\right) \tag{78}$$

$$= \frac{k_BT\,\Theta}{(2\pi)^2 A} 2\mathrm{Re}\left\{\Gamma_{\mathbf{k}}(\omega)\right\} , \tag{79}$$

where we have used the fact that $\hat{\gamma}_{\mathbf{k}}(\omega)^* = \hat{\gamma}_{\mathbf{k}}(-\omega)$.

With the present definition of the Fourier transform the Wiener-Khintchine relation for the velocity autocorrelation function reads

$$\langle \dot{h}_{\mathbf{k}}(t)\dot{h}^*_{\mathbf{k}}(0)\rangle = \frac{2\pi}{\Theta}\int_{-\infty}^{\infty} d\omega\, e^{-i\omega t}|\hat{\dot{h}}_{\mathbf{k}}(\omega)|^2 , \tag{80}$$

which by Eq. (78) takes the form

$$\langle \dot{h}_{\mathbf{k}}(t)\dot{h}^*_{\mathbf{k}}(0)\rangle = \frac{k_BT}{2\pi A}\int_{-\infty}^{\infty} d\omega\, (e^{-i\omega t} + e^{i\omega t})\,\Gamma_{\mathbf{k}}(\omega) \tag{81}$$

where the substitution $\omega \to -\omega$ has been used in the last term. Since $\Gamma_{\mathbf{k}}(\omega)$ has no poles in the upper half plane, it follows that when $t > 0$ ($t < 0$) a contour can be closed in the upper half plane for the integration of the second (first) term and only the first (second) term contributes. We can thus write

$$\langle \dot{h}_{\mathbf{k}}(t)\dot{h}^*_{\mathbf{k}}(0)\rangle = \frac{k_BT}{2\pi A}\int_{-\infty}^{\infty} d\omega\, e^{-i\omega|t|}\Gamma_{\mathbf{k}}(\omega) \tag{82}$$

as the final form for the velocity autocorrelation function.

We now identify the time dependence in this expression as that of a macroscopic perturbation of the interface. Observing that Eq. (67) describes not only the dynamic response to fluctuations, but also the response to an external force, we replace $\tilde{F}$ with $\hat{G}_{\mathbf{k}}(\omega) = \frac{G_{0k}}{2\pi}$. This corresponds to having a force $G_{\mathbf{k}}(t) = G_{0k}\delta(t)$ acting on the interface, thus adding the momentum G_{0k} to the system at time $t = 0$. The resulting velocity $\dot{h}_{\mathbf{k}}(t)$ is given by Eq. (67) as

$$\dot{h}_{\mathbf{k}}(t) = \frac{G_{0k}}{2\pi}\int_{-\infty}^{\infty} d\omega\,\Gamma_{\mathbf{k}}(\omega)e^{-i\omega t} . \tag{83}$$

By normalizing the autocorrelation function in Eq. (82) and the decaying velocity above by their respective values at $t = 0$ we find that

$$\frac{\langle \dot{h}_{\mathbf{k}}(t)\dot{h}^*_{\mathbf{k}}(0)\rangle}{\langle |\dot{h}_{\mathbf{k}}(0)|^2\rangle} = \frac{\dot{h}_{\mathbf{k}}(|t|)}{\dot{h}_{\mathbf{k}}(0)} , \tag{84}$$

which is the statement that the fluctuations, when averaged to a correlation function, decay according to the hydrodynamic response of the system. In other words, a microscopic, spontanous thermal fluctuation decays, on the average, with exactly the same time dependence as does a macroscopic perturbation of the system. In the present context, this result has been derived from the starting point of fluctuating hydrodynamics and the corresponding uncorrelated body force f in the bulk of the fluids, via the correlation function for the force $\tilde{F}_{\mathbf{k}}(t)$ on the interface. If Eqs. (84) and (67) had instead been taken as the starting point, the correlation function for the force $\tilde{F}_{\mathbf{k}}(t)$ could have been obtained (up to the prefactor k_BT giving the strength of the thermal excitations in the fluids). When the hydrodynamic description in Eq. (67) is given, the various forms of the fluctuation-dissipation theorem thus contain the same information.

The power spectrum for the height $|\hat{h}_{\mathbf{k}}(\omega)|^2$ is easily obtained from Eq. (79) by the substitution $|\hat{\dot{h}}_{\mathbf{k}}(\omega)|^2 = \omega^2|\hat{h}_{\mathbf{k}}(\omega)|^2$, in which case we get

$$|\hat{h}_{\mathbf{k}}(\omega)|^2 = \frac{\Theta}{(2\pi)^2}\frac{k_BT}{\omega^2 A} 2\mathrm{Re}\{\Gamma_{\mathbf{k}}(\omega)\} . \tag{85}$$

This power spectrum has the same form as that found by Herpin and Meunier [34] in the more general case where the fluids have different densitites and viscosities.

The correlation function corresponding to Eq. (85) reads

$$\langle h_{\mathbf{k}}(t)h^*_{\mathbf{k}}(0)\rangle = \frac{k_BT}{2\pi A}\int_{-\infty}^{\infty}\frac{d\omega}{\omega^2} e^{-i\omega|t|}\Gamma_{\mathbf{k}}(\omega) . \tag{86}$$

This integral is evaluated in the long-time, low viscosity limit in Appendix B using the integration contour shown in Fig. 4. The result is

$$\langle h_{\mathbf{k}}(t)h^*_{\mathbf{k}}(0)\rangle = \langle h_{\mathbf{k}}(t)h^*_{\mathbf{k}}(0)\rangle_{\mathrm{CW}} + \langle h_{\mathbf{k}}(t)h^*_{\mathbf{k}}(0)\rangle_{\mathrm{cut}} \tag{87}$$

where the two last terms correspond to the capillary waves, and the C_{cut} part of the contour shown in Fig. 4, respectively. When the values of the viscosity and surface tension are such that oscillating (as opposed to overdamped) capillary waves of wave number k exist, we obtain

$$\langle h_{\mathbf{k}}(t)h^*_{\mathbf{k}}(0)\rangle_{\mathrm{CW}}$$

$$= \frac{k_BT}{\sigma k^2 A}\left(\cos(\omega_r|t|) - \frac{\omega_i}{\omega_r}\sin(\omega_r|t|)\right) e^{-\omega_i|t|} , \tag{88}$$

where ω_r and ω_i are the absolute values of the real and imaginary parts of the capillary wave poles shown in Fig. 4. The contribution from the "cut" part of the contour is less trivial to evaluate. In the long-time limit it has the asymptotic form

$$\langle h_{\mathbf{k}}(t)h_{\mathbf{k}}(0)\rangle_{\mathrm{cut}} = \frac{2k_BT}{k^4 A\sigma^2}\frac{\rho\nu^{1/2}}{}\frac{e^{-k^2\nu|t|}}{|t|^{3/2}} , \tag{89}$$

which together with Eq. (88) gives the long-time limit of the height autocorrelation function.

There is an ambiguity concerning the treatment of the $\omega = 0$ pole. The contour of Fig. 4 is chosen so that the pole at $\omega = 0$ (giving a time-independent contribution) is not included. Consequently the height correlation function vanishes at $t \to \infty$. However, when $t = 0$ the contour can be closed in the upper half plane. As a result, the contribution to the Fourier integral from the pole at $\omega = 0$ is identified as the equilibrium variance of the height and is given as

$$\langle |h_{\mathbf{k}}(0)|^2\rangle = \frac{k_BT}{\sigma A k^2} . \tag{90}$$

The physical content of this result is that of equipartition of surface energy: The surface energy is here the potential energy given as $\sigma\times$(area of interface) [35]. When this energy is written out in terms of the Fourier modes $h_{\mathbf{k}}$ it takes the form of a sum over terms which are quadratic in $h_{\mathbf{k}}$ in the small-height-gradient limit. Equation (90) results when each of these terms is given an energy $k_BT/2$.

In order to investigate the importance of the correlations in $\tilde{F}_{\mathbf{k}}(t)$ we also give the power spectrum in the case where $\langle \tilde{F}^*_{\mathbf{k}}(t)\tilde{F}_{\mathbf{k}}(0)\rangle \propto \delta(t)$. This assumption is made by Yang [36] who obtains an approximate form of Eq. (67). In the case of uncorrelated forces, $|\hat{\tilde{F}}_{\mathbf{k}}|^2 \propto \Theta$ and Eq. (85) takes the form

$$|\hat{h}_Y(\omega)|^2 = \frac{4k\nu\Theta}{(2\pi)^2 A\omega^2}|\Gamma_{\mathbf{k}}(\omega)|^2, \tag{91}$$

where the prefactor is identified by comparison with Eq. (85) and the requirement that the spectra be equal in the $\omega = 0$ limit. Alternatively, this identification could have been done using the fluctuation-dissipation relation for the uncorrelated force or by integration over all ω to get $\langle |h_{\mathbf{k}}|^2\rangle$ and the use of equipartition. By using the definitions of $\Gamma_{\mathbf{k}}$, $\gamma_{\mathbf{k}}$, and q it is possible to work out the ratio

$$\frac{|\hat{h}(\omega)|^2}{|\hat{h}_Y(\omega)|^2} = \frac{1}{2}\left[1 + \frac{1}{\sqrt{2}}\left[1 + \left[1 + \left(\frac{\omega}{k^2\nu}\right)^2\right]^{1/2}\right]^{1/2}\right] \tag{92}$$

$$\approx \begin{cases} 1 + \left(\frac{\omega}{4k^2\nu}\right)^2 & \text{when } \frac{\omega}{k^2\nu} \ll 1 \\ \frac{1}{2} + \left(\frac{\omega}{8k^2\nu}\right)^{1/2} & \text{when } \frac{\omega}{k^2\nu} \gg 1. \end{cases} \tag{93}$$

It is seen that the two spectra agree in the low frequency limit. But in the high frequency limit they differ qualitatively. The physical reason for this is that it is always possible (at least in principle) to probe the system at frequencies high enough for the correlations in the force $\tilde{F}$ to be important. Note that the ratio does not depend on the surface tension, but only on the ratio of ω to the viscous diffusion time. An alternative view of this

problem in a weakly out-of-equilibrium context has been considered by Grant and Desai [37].

Finally, we note an interesting comparison with the long-time power-law decay of correlations in Brownian motion [9]. The exponential, rather than algebraic, decay in Eq. (89) corresponds to the fact that the correlated interface motion is given in terms of Fourier modes, each with a given wavelength $2\pi/k$. The flow field associated with each mode thus has a characteristic length, and the viscous decay of the corresponding momentum takes place within a volume given by this fixed length. There is a cancellation of momentum in the interface case. The volume integrated momentum related to a perturbation $\dot{h}_{\mathbf{k}}$ of the interface vanishes whereas the corresponding integrated momentum related to a fluctuation of the velocity $\mathbf{U}$ of the Brownian particle does not. Hence, while the momentum related to $\dot{h}_{\mathbf{k}}$ will decay when it has diffused a length $2\pi/k$, the momentum related to $\mathbf{U}$ must diffuse away to infinity in order to decay. The slow algebraic decay of this motion results because the shear forces in the flow become sufficiently weak as the spatial extension of the flow field increases.

VI. THE ROUGHENING INTERFACE

Having obtained the description of the equilibrium fluctuations in terms of the power spectrum and correlation function, we now turn to the description of the roughness and the roughening of an initially flat interface.

We shall be concerned with the root-mean-square interface width W, which is defined by

$$W^2(t) = \left\langle \frac{1}{A} \int dS\, h^2(\mathbf{x},t) \right\rangle , \tag{94}$$

where $h(\mathbf{x},t)$ is real and the other quantities are as in Fig. 1. We shall derive the time evolution of the Fourier components in the low viscosity limit, before we obtain $W(t)$, from this result and Eq. (90), in the limits of small and large t.

In terms of the spatial Fourier transform, Eq. (94) takes the form

$$W^2(t) = \frac{1}{2} \sum_{\mathbf{k}} \langle |h_{\mathbf{k}}(t)|^2 \rangle , \tag{95}$$

where we have now taken $h_{\mathbf{k}}(t)$ to be the Fourier transform of a complex $h(x,t)$. The factor $1/2$ is included to compensate for this.

In order to obtain the time dependence of W, we shall assume that the interface is driven by a fluctuating force which vanishes for $t < 0$ and use the approximation that this force immediately assumes its equilibrium correlations, as given in Eq. (61).

The starting point will be Eq. (67) written in the Fourier transformed form

$$h_{\mathbf{k}}(t) = \frac{1}{2\pi} \int_0^\infty ds\; R_{\mathbf{k}}(t-s)\; G_{\mathbf{k}}(s), \tag{96}$$

where the response function $R_{\mathbf{k}}$ is

$$R_{\mathbf{k}}(t) = \int_{-\infty}^{\infty} d\omega\; \frac{i}{\omega} \Gamma_{\mathbf{k}}(\omega) e^{-i\omega t} . \tag{97}$$

The force $G_{\mathbf{k}}(t) = \tilde{F}_{\mathbf{k}}(t)$ when $t > 0$ and $G_{\mathbf{k}}(t) = 0$ when $t \le 0$.

The autocorrelation function for $G_{\mathbf{k}}(t)$ given by the fluctuation-dissipation theorem, Eq. (61), will appear to be divergent as $1/t^{3/2}$ at $t = 0$. Mathematically, the divergence arises from the high frequency limit of the corresponding Fourier integral. Since a precise physical description of any system should, in principle, always contain an upper frequency cutoff, this means that the divergence could be removed by introducing such a cutoff.

For mathematical tractability we shall, however, keep the infinite integration limits and instead introduce a proper regularization step in the calculations. Also, we shall evaluate the Fourier integrals only in the $\nu \to 0$ limit. For the simulations this can be justified to some extent by the fact that the viscous relaxation time $(k^2\nu)^{-1}$ is larger than the capillary wave period even for the smallest wavelengths on the lattice.

Upon squaring Eq. (96) we can write

$$\begin{aligned} \langle |h_{\mathbf{k}}(t)|^2 \rangle &= \int_0^\infty \frac{ds\,ds'}{(2\pi)^2} R_{\mathbf{k}}(t-s) R^*_{\mathbf{k}}(t-s') \langle \tilde{G}_{\mathbf{k}}(t) \tilde{G}^*_{\mathbf{k}}(0) \rangle \\ &= \frac{2k_BT}{A} \int_0^\infty \frac{ds\,ds'}{(2\pi)^2} R_{\mathbf{k}}(t-s) R^*_{\mathbf{k}}(t-s') \\ &\quad \times \gamma_{\mathbf{k}}(|s-s'|), \end{aligned} \tag{98}$$

where the response functions $\gamma_{\mathbf{k}}$ and $R_{\mathbf{k}}$ remain to be evaluated. As $\nu \to 0$, $k/q \to 0$ and $\gamma(t)$ is given by the Dirac δ function in Eq. (65). When these replacements are made in Eq. (97) we obtain the integral

$$R_{\mathbf{k}}(t) = \frac{k}{2\rho} \int_{-\infty}^{\infty} d\omega\; \frac{e^{-i\omega t}}{\omega^2 - \frac{\sigma}{2\rho} k^3}, \tag{99}$$

which is easily evaluated for $t > 0$ by enclosing the two poles at $\omega = \pm\omega_0$ by a contour in the lower half ω plane. For $t < 0$ a contour can be closed in the upper half plane, giving $R_{\mathbf{k}}(t < 0) = 0$. In other words, the response function $R_{\mathbf{k}}(t)$ is causal, as one would expect. The result for $t > 0$ is

$$R_{\mathbf{k}}(t) = \frac{k\pi}{\rho\omega_0} \sin(\omega_0 t), \tag{100}$$

where ω_0 is given in Eq. (70). Combining Eqs. (98) and (100) and the zero viscosity limit of $\gamma_{\mathbf{k}}(t)$ we get

$$\begin{aligned} \langle |h_{\mathbf{k}}(t)|^2 \rangle = \frac{2k_BT}{\sigma k^2 A} \int_0^t ds 2 \int_0^{s_+} ds' \sin[\omega_0(t-s)] \\ \times \sin[\omega_0(t-s')]\, \delta'(s-s') , \end{aligned} \tag{101}$$

where the factor 2 in front of the last integral comes from the restriction $s' \le s_+$. The introduction of the integration limit $s_+ > s$ represents the above mentioned regularization. In the end the $s_+ \to s$ limit is implied, but it is crucial that this limit is taken after the s' in-

tegration is performed, as this integration will pick up the contribution from the delta function δ'. After the s' integration Eq. (101) takes the simple form

$$\begin{aligned}\langle|h_{\mathbf{k}}(t)|^2\rangle &= \frac{4k_BT\omega_0}{\sigma k^2 A}\int_0^t ds\,\sin[\omega_0(t-s)]\cos[\omega_0(t-s)] \\ &= \frac{2k_BT\omega_0}{\sigma k^2 A}\int_0^t ds\,\sin[2\omega_0(t-s)] \\ &= \frac{2k_BT}{\sigma k^2 A}\sin^2(\omega_0 t)\ . \end{aligned} \tag{102}$$

By taking the time average of Eq. (102), the equipartition result given in Eq. (90) is recovered. The factor $2\sin^2(\omega_0 t)$ describes standing capillary waves that are all initiated with the same (vanishing) phase and have frequencies given by the inviscid dispersion relation (70). Hence, Eq. (102) could have been written down from the simple physical prescription that the interface will roughen by the motion of preexcited capillary waves, with amplitudes distributed according to the equipartition theorem. This picture is not surprising in view of the assumption that the fluctuating forces instantaneously assume their equilibrium correlations. In fact, this assumption would follow if flat interfaces were considered a spontaneous state of the system. In this case the further dynamics of the interface would clearly be governed by equilibrium statistics. In the following we compute the form of $W(t)$ that results from Eqs. (102) and (90) in the general case of an interface contained in a d-dimensional space of linear size L in all directions except possibly in the direction perpendicular to the interface.

A. The steady state

First we obtain the equilibrium interface width W. Introducing the length a, which is the smallest wavelength available for the system, we note that there is an upper cutoff for the wave number, i.e., $k < 2\pi/a$, and a corresponding cutoff for the components of $\mathbf{n}$, $n_{\max} = L/a$. The length a can be taken as the scale at which the hydrodynamic description breaks down for a real system or the lattice constant in a simulation. It cannot be given a meaningful exact value, and it is therefore important to verify, where possible, that the end results are a independent.

From Eq. (90) we can write

$$\begin{aligned} W^2 &= \sum_{\mathbf{k}} \frac{k_BT}{\sigma k^2 L^{(d-1)}} \\ &= L^{(3-d)} \sum_{\mathbf{n}\,:\,n<L/a} \frac{k_BT}{\sigma(2\pi\mathbf{n})^2}\ , \end{aligned} \tag{103}$$

where the sum is over the $(d-1)$-dimensional k space and the substitution $k_i = 2\pi n_i/L$ where $n_i = \pm1, \pm2, \ldots$ and i is a Cartesian index, has been used in the second line. This sum can be approximated by an integral to evaluate the high k contribution. The integrand that results from doing the integration in polar coordinates will contain a geometric prefactor of the form $k^{(d-2)}$. When $d = 2$ the $a \to 0$ limit of the sum exists, and for finite values of a the relative correction to the asymptotic result is $o(a/L)$. When $d = 3$ the sum will increase logarithmically with L/a, and when $d > 3$ the high wave numbers dominate completely and the L dependence goes away. Using the exact relation $\sum_{n=1}^{\infty} 1/(2\pi n)^2 = 1/24$, Eq. (103) takes the form

$$W^2 = \frac{k_BT}{\sigma} \times \begin{cases} \frac{1}{12}L, & d=2 \\ \ln\left(\frac{L}{a}\right), & d=3 \\ a^{(3-d)}, & d>3, \end{cases} \tag{104}$$

where the exact numerical prefactors are included only in the $d = 2$ results.

B. Nonequilibrium roughening

We now turn to the derivation of $W(t)$ for small and finite t. From Eqs. (95) and (102) we can write

$$W^2(t) = \sum_{\mathbf{n}\,:\,n_i<L/a} \frac{2k_BT}{\sigma k_{\mathbf{n}}^2\, L^{(d-1)}}\ \sin^2(\omega_{0\mathbf{k}}t)\ . \tag{105}$$

As before, the limit $a \to 0$ is meaningful only in the two-dimensional case. Using the explicit form for ω_{0k} given in Eq. (70), the above expression can be cast in the scaling form

$$W^2(t) = \begin{cases} L\, f(t/L^{3/2}), & d=2 \\ \frac{1}{L^{(d-3)}}\, g\left(\frac{L}{a}, \frac{t}{L^{3/2}}\right), & d \geq 3, \end{cases} \tag{106}$$

where the $d = 2$ scaling function has the explicit form

$$f(u) = \sum_n \frac{k_BT}{\sigma(\pi n)^2}\ \sin^2\left(\sqrt{\frac{\sigma}{2\rho}}(2\pi n)^{3/2}u\right)\ . \tag{107}$$

This function, which is obtained in the $\nu = 0$ limit, retains its oscillatory behavior for arbitrarily large t. For this reason, it does not describe the asymptotic state of the interface, where the initial phases have been randomized and the interface has reached its final width. This randomization, which is caused by the dissipative decay of the initial excitations, is present only when $\nu \neq 0$.

For small times the roughening of the interface will be dominated by the shortest wavelengths. This can be seen by comparing the values of $|\dot{h}_{\mathbf{k}}(t)|^2 \sim \omega_{0\mathbf{k}}^2|h_{\mathbf{k}}|^2 \sim \omega_{0\mathbf{k}}^2/k^2 \sim k$ derived from Eq. (102) for different wave numbers. The long waves with smaller wave numbers grow at a slower rate than the shorter waves by a relative factor $\sqrt{k}$. When $d > 2$ the domination of the high wave numbers will be enhanced by the higher density of states with large k. Hence initially W cannot depend on the system size L, and in the two-dimensional case the scaling function $f(u)$ must have the form

$$f(u) \sim u^{2/3} \tag{108}$$

for small u, in order to make the right hand side of Eq. (106) L independent for small t. This simple argument cannot be used, however, to determine the scaling

function g. Hence, as will become evident below, only the time dependence of the interface in $d = 2$ is described by a power law.

In order to obtain a closed form expression for $W^2(t)$ in $d = 2$ and the time dependence that follows from Eq. (105) when $d > 2$, we approximate the sum by an integral. Changing to polar coordinates in the integral this gives

$$W^2(t) = \frac{k_B T}{\sigma} \int \frac{d^{d-1}\, k}{(2\pi)^{d-1}} \frac{2\sin^2 \omega_0 t}{k^2} = \frac{k_B T}{\pi\sigma} \int_0^{2\pi/a} dk\; k^{d-4} \sin^2(\omega_{\mathbf{k}} t), \tag{109}$$

where again the prefactor is correct only for $d = 2$. By the substitution $x = \omega_{\mathbf{k}} t$ this integral takes the form

$$W^2(t) = \frac{2k_B T(2\rho)^{d/3-1}}{3\pi\sigma^{d/3}} t^{2-2d/3} \int_0^{\omega_a t} dx \frac{\sin^2 x}{x^{(3-2d/3)}}, \tag{110}$$

where ω_a is the frequency of the capillary wave with wavelength a. When $d = 2$ and the dependence on the upper integration limit becomes negligible, the above time dependence is a simple power law, whereas when $d > 2$ the time dependence also depends on the time scale $1/\omega_a$, and is more complex. When $d = 3$ the prefactor in Eq. (110) becomes time independent, and only the time dependence contained in the integral $W^2(t) \sim \ln \omega_a t$ for $t > 1/\omega_a$ remains. When $d > 3$ the interface reaches its asymptotic width on a time scale ω_a^{-1}, and there is no long-time evolution.

It can be shown that the relevant integral for $d = 2$,

$$I = \int_0^\infty dx\, \frac{\sin^2 x}{x^{5/3}} = \frac{\pi}{2^{1/3}\sqrt{3}\,\Gamma(5/3)} = 1.5947..., \tag{111}$$

where Γ is the usual Gamma function. The resulting dynamic behavior for $t > \omega_a^{-1}$ can thus be written

$$W^2(t) = \begin{cases} \frac{2^{1/3}}{3^{3/2}\,\Gamma(5/3)} \frac{k_B T}{(\rho\sigma^2)^{1/3}}\, t^{2/3} & \text{when } d = 2 \\ \frac{k_B T}{\sigma} \ln(\omega_a t) & \text{when } d = 3 \\ \text{const} & \text{when } d > 3. \end{cases} \tag{112}$$

As previously mentioned, the crossover between the short- and long-time behavior depends on correlations in the system that build up over time. The exact time for this to happen cannot be read out of Eq. (102), since this equation is obtained in the zero viscosity limit where the force becomes uncorrelated. However, a crude estimate of the crossover time t_c can be obtained by assuming that $W(t)$ grows until the longest capillary wave has reached its maximum amplitude. The corresponding time for this to happen is $t_c = T/4$, where the period $T = 2\pi/\omega_0$ is estimated by the inviscid disperson relation Eq. (70), using $k = 2\pi/L$. This gives the result

$$t_c = \sqrt{L^3\rho/(16\pi\sigma)}\,. \tag{113}$$

The L dependences in the $d = 2$ and $d > 2$ cases are in marked contrast. In two dimensions W depends on L as the root-mean-square distance of a random walk depends on time. In three dimensions, W depends very weakly on L, and the numerical value of W is correspondingly small: If a is taken to be the typical width of an atom, and L the width of the earth, the factor $\sqrt{\ln(L/a)}$ is still less than 7. If σ is taken to have some characteristic value, say the surface tension between water and cyclohexane, $\sigma \approx 0.03$ N/m, and T to be room temperature, the prefactor $\sqrt{k_B T/\sigma}$ is only 2 Å.

However, in both two and three dimensions the roughening time t_c, given by the growth time of the longest capillary wave in the system, is relatively large. For $d = 3$ and the above values of σ and T, $L = 10$ cm, and $\rho = 1000$ kg/m^3, we get the value $t_c \approx 5$ s for the crossover time. On the other hand, if the smallest wavelength available to the system is chosen as $a = 100$ Å, we have that the time scale corresponding to the high frequency cutoff $2\pi/\omega_a \approx 10^{-10}$ s. Hence Eq. (112) is expected to hold over approximately ten orders of magnitude in the time domain.

A study which has a somewhat similar aim as the present one has been carried out by Kuhn [5] who considers the growth due to thermal motion of a given perturbation on the interface of a stationary cylindrical body of fluid. The perturbation is taken to have a Gaussian shape, and the study is based on the essentially unqualified assumption that the effect of correlations can be neglected. Consequently, Kuhn assumes that the amplitude of the perturbation varies like the position of a random walk, i.e., that it grows as $t^{1/2}$, in contrast with the result of Eq. (112).

VII. SIMULATIONS

We now turn to numerical simulations of fluctuating fluid interfaces. We use the immiscible lattice gas [20], a variant of the now classical Frisch-Hasslacher-Pomeau (FHP) lattice gas [18], to simulate two fluctuating two-dimensional fluids of equal densities and equal viscosities separated by an interface with surface tension σ. We choose to employ a lattice-gas model for several reasons. First, compared with molecular dynamics, a lattice-gas model allows one to bridge the microscopic and macroscopic scales of hydrodynamics efficiently by discretization of particle dynamics. Second, although one could add interfacial tension and a fluctuating stress tensor to a finite-difference approximation of the Navier-Stokes equations, the microscopic nature of the lattice gas allows statistical noise—and therefore hydrodynamic fluctuations—to emerge naturally from the dynamics, rather than being engineered into a model. Lastly, we feel that the lattice-gas model is the simplest possible way to investigate fluctuating interfaces. We shall see, however, that a cost of this simplicity is an ambiguity in the pertinent value of $k_B T$.

Below, we first provide a brief review of the immiscible lattice gas. We then describe the numerical experiment itself, and compare the equilibrium and nonequilibrium behavior of the immiscible lattice gas with the theory developed in the preceding sections.

A. The immiscible lattice gas

The immiscible lattice gas (ILG) [20] and related models of hydrodynamic interfaces have been the subject of a recent review [21], so our discussion here will be brief.

The basic two-dimensional lattice-gas model [18,19,21] consists of a collection of identical particles moving from site to site on a hexagonal lattice with one of six possible velocities. When particles meet at a site, they collide in a manner that can result in a change in their velocity, but not the total momentum. From the conservation of mass and momentum at this microscopic scale, and from symmetry properties of the hexagonal lattice, macrodynamics very close to the Navier-Stokes equations may be derived using the methods of kinetic theory [18,19,22–24].

The ILG retains the simplicity of the original lattice gas but with two additional complications. First, there are now two types of particles, "red" and "blue." Second, the collision rule conserves an additional quantity (say, the number of red particles) and is designed to create interfaces and surface tension.

Figure 5 illustrates the ILG microdynamics, which consist of successive iterations of a propagation or free-streaming step followed by a collision step. Figure 5(a) shows an abritrary initial condition, followed by the motion of each particle in the direction of its velocity to the neighboring lattice site [Fig. 5(b)]. The collision step in Fig. 5(c) creates interfaces and surface tension. Broadly speaking, the ILG collision changes the configuration of particles so that, as much as possible, red particles are directed towards neighbors containing red particles, and blue particles are directed towards neighbors containing blue particles. The total mass, the total momentum, and the number of red (or blue) particles are conserved. Two examples of this collision rule are seen by comparing the middle row of Fig. 5(b) with that of Fig. 5(c).

More specifically, the ILG microdynamics may be described as follows. Each lattice site may contain red particles, blue particles, or both, but at most one particle (red or blue) may move in each of the six directions $\mathbf{c}_1, \ldots, \mathbf{c}_6$. In this implementation, each site also has a seventh stationary, or rest, particle with zero velocity $\mathbf{c}_0$ and subject to the same exclusion rule. The configuration at a site $\mathbf{x}$ is thus described by the Boolean variables $\mathbf{r} = \{r_i\}$ and $\mathbf{b} = \{b_i\}$, where the index i again indicates the velocity, and r_i and b_i cannot simultaneously equal 1.

At a site $\mathbf{x}$, a color flux $\mathbf{q}$ is defined to be the difference between the red momentum and the blue momentum:

$$\mathbf{q}(\mathbf{r}(\mathbf{x}), \mathbf{b}(\mathbf{x})) \equiv \sum_{i=1}^{6} \mathbf{c}_i [r_i(\mathbf{x}) - b_i(\mathbf{x})]. \tag{114}$$

A vector proportional to the local color gradient is also defined, by

$$\mathbf{f}(\mathbf{x}) \equiv \sum_i \mathbf{c}_i \sum_j [r_j(\mathbf{x} + \mathbf{c}_i) - b_j(\mathbf{x} + \mathbf{c}_i)]. \tag{115}$$

The ILG collision rule maximizes the flux of color in the direction of the local color gradient. In other words, the result of a collision, $\mathbf{r} \to \mathbf{r}'$, $\mathbf{b} \to \mathbf{b}'$, is the configuration that maximizes

$$\mathbf{q}(\mathbf{r}', \mathbf{b}') \cdot \mathbf{f}, \tag{116}$$

such that the number of red particles and the number of blue particles are conserved,

$$\sum_{i=0}^{6} r_i' = \sum_{i=0}^{6} r_i, \qquad \sum_{i=0}^{6} b' = \sum_{i=0}^{6} b_i, \tag{117}$$

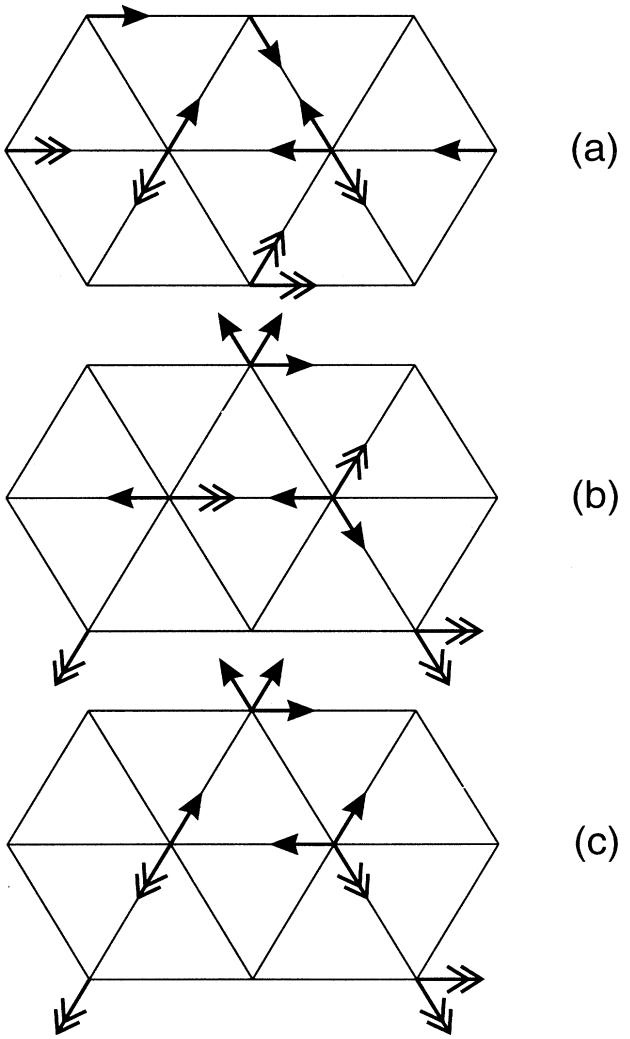

FIG. 5. Microdynamics of the immiscible lattice gas [21], in which the initial condition (a), the propagation step (b), and the collision step (c) are displayed. The initial condition and propagation step are the same as before, except that now some particles are red (bold arrows) while others are blue (double arrows). In the collision step, the particles are rearranged so that, as much as possible, the flux of color is in the direction of the local gradient of color. The ILG collisions can create a "color-blind" microdynamics different from that created by FHP collisions.

as is the total momentum:

$$\sum_i \mathbf{c}_i(r_i' + b_i') = \sum_i \mathbf{c}_i(r_i + b_i). \tag{118}$$

If more than one choice for $\mathbf{r}'$ and $\mathbf{b}'$ maximizes (116), then the outcome of the collision is chosen with equal probability from among this set of configurations.

From a physical perspective, it is intuitively evident from the ILG collision rules that the dynamics can be antidiffusive; i.e., color can travel up the color gradient. This is the mechanism that creates interfaces if the model is initialized as a random mixture. Further analysis [21,29] shows that surface tension is created at the interface due to anisotropy in the local pressure tensor.

It is important to note that the particle interactions described above are such that some input configurations can never appear as output configurations. Hence the interactions do not satisfy detailed balance (or, in other words, the microdynamics are time irreversible). Also, the particle dynamics do not satisfy energy conservation. For these two reasons we shall only work with an effective temperature $k_B T_{\text{eff}}$, describing the effective strength of the excitations of the interface, and not, as do other authors [38], obtain this temperature theoretically in terms of the stress fluctuations in the lattice gas. Below, however, we demonstrate that the concept of an effective temperature is consistent by comparing the nonequilibrium and equilibrium values obtained for $k_B T_{\text{eff}}$.

B. The numerical experiment and comparison with theory

Simulations where carried out on lattices of size $N \times N$, with two completely separated phases of equal area and the interface oriented in a direction perpendicular to a lattice direction. Hence the flattest possible interface (on the triangular lattice) has an initial width $W = 1/4$. The location of the interface, and thus the height function $h(x_j, t), j = 1, ..., N$, was determined using the scheme described in Ref. [29].

The Fourier transforms of the (discrete) simulation data are defined as follows:

$$h_k(t) = \frac{1}{N} \sum_j e^{-ikx_j} h(x_j, t), \tag{119}$$

$$\hat{h}_k(\omega) = \frac{1}{2\pi} \sum_j e^{-ikt_j} h_k(t_j), \tag{120}$$

where $x_j = (\sqrt{3}/2)j$, $j = 1, ..., N$, and $t_j = j$, $j = 1, ..., \Theta$. The wave numbers and frequencies are given as $k = (2\pi/L)n$, $n = \pm 1, ..., \pm N/2$, and $\omega = (2\pi/\Theta)n$, $n = \pm 1, ..., \pm\Theta/2$. The above definitions are the discrete equivalents of the definitions given in Eqs. (17) and (19), and we shall make direct comparisons between the continuous transforms of the theory and the transforms of the simulation data which are performed using Eqs. (119) and (120).

The relevant material properties of the ILG simulations,

$$\begin{aligned} \nu &= 0.2357, \\ \sigma &= 0.403, \\ \rho &= 4.9, \\ k_B T_{\text{eff}} &= 0.126\,, \end{aligned} \tag{121}$$

are all given in units which are combinations of the lattice constant and the simulation time step. These quantities are set to 1. Hence the above quantities appear dimensionless. The first two quantities are obtained by theoretical analysis [21], and depend only on the density ρ. While the theoretical prediction for ν is reliable, the prediction for σ has a relative accuracy that is probably no better than 10%. The temperature, which also depends on the density, is the only free parameter in the simulations.

Frequency power spectrum

In Fig. 6(a), the power spectrum $|\hat{h}_{\mathbf{k}}(\omega)|^2$ for the simulated interface in equilibrium is shown on a log-log plot along with the theoretical prediction given by Eq. (85). This frequency spectrum was computed from a consecutive series of $2^{20} \approx 10^6$ interfaces with $N = 32$. Each data point results from the average over bins of at least 512 frequency values. The effective temperature kT_{eff} was chosen to minimize the difference between theory and simulation.

Theoretically, there are three significant features in the power spectra. First, there is the peak at ω_0 corresponding to the capillary wave of wave number k. Then, there is the plateau to the left of this peak, showing significant low frequency behavior over one to two orders of magnitude. Finally, there is the $1/\omega^{7/2}$ decay at high frequencies. Each of these properties predicted by theory is captured by the ILG, with agreement spanning over three orders of magnitude on the vertical axis. However, a clear departure from the theoretical predictions is observed above the frequency c_s/H, where $c_s = \sqrt{3/7}$ is the speed of sound in the ILG [21] and $H = N$ is the height of the box. For the smallest wave number, the peaks of the three first standing sound waves of the system are visible. These have wavelengths H, $H/2$, and $H/3$, respectively. The height of the system is the relevant length, because the sound waves creating distortions in the interface height have wave vectors perpendicular to the interface. By doing the simulations in systems of greater height, it was checked that there was no significant H dependence in the low frequency behavior. The high frequency ($\omega > 2\pi c_s/H$) behavior of the power spectrum obtained from simulations,

$$|h(\omega)|^2 \sim 1/\omega^{\alpha} \text{ where } 1.0 < \alpha < 1.2, \tag{122}$$

may be a consequence of compressibility effects in the lattice gas, and could possibly be explained by a Landau-Placzek type theory [25]. The low frequency plateau of the power spectrum diminishes and the peak at the capillary wave frequency becomes more pronounced when $k^2\nu$ is decreased. At large $k^2\nu$ the dominant small-frequency

behavior is caused by the fact that in a thick fluid the relaxation of the interface is relatively slow.

Figure 6(b), which shows the result of an $N = 96$ simulation along with the two theoretical results Eqs. (85) and (91), is included to quantify the effect of correlations in $\tilde{F}$ in the simulations. The effective k_BT which is taken as input in Eq. (85) is the same as that used in Fig. 6. The effective temperature used in Eq. (91) is chosen so as to obtain agreement with the simulations in the low frequency regime where the uncorrelated theory is expected to work best.

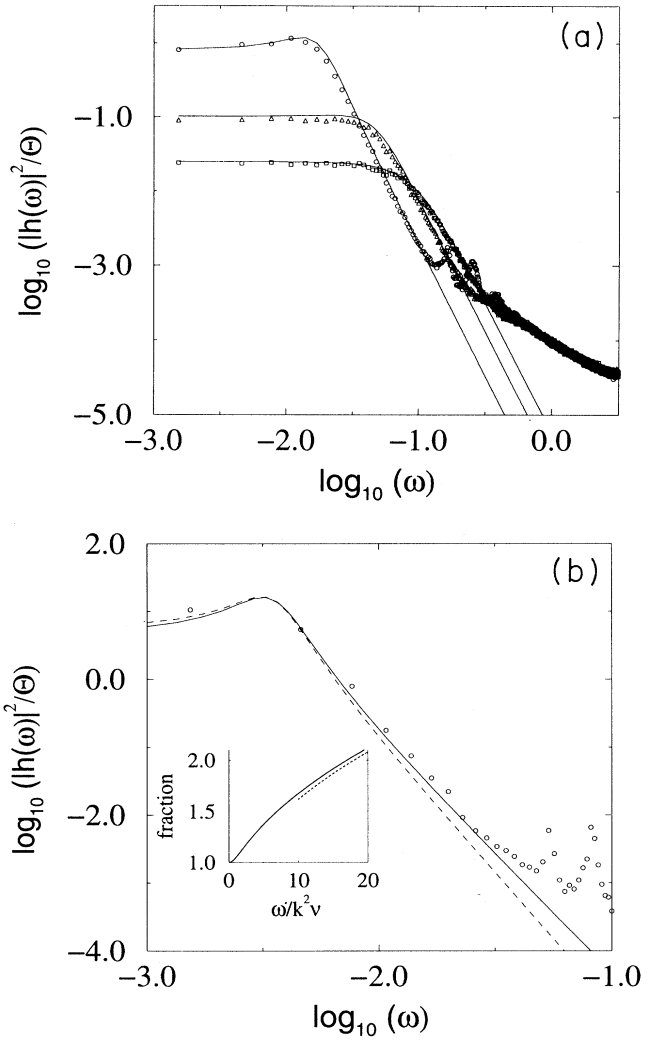

FIG. 6. (a) The power spectrum $|\hat{h}_k(\omega)|^2/\Theta$ for the wave numbers $k = 2\pi/L$, $k = 4\pi/L$, and $k = 6\pi/L$; $N = 32$. The solid lines show the theory, Eq. (85), and the circles, triangles, and squares show the results of simulations for large to small wavelengths, respectively. The same effective temperature was used for all three theoretical curves. (b) The power spectrum for $k = 2\pi/L$ and $N = 96$. The circles show simulations, the straight line the theory given by Eq. (85), and the dashed line the theory given in Eq. (91) corresponding to uncorrelated interface forces. The inset shows the ratio of the power spectrum corresponding to a correlated force given in Eq. (85) to the spectrum corresponding to an uncorrelated force given in Eq. (91). The dashed line shows the high frequency approximation in Eq. (93) of the ratio of the power spectra.

The inset of Fig. 6(b) shows the ratio, which is given in Eq. (92), of the power spectra corresponding to a correlated and an uncorrelated force, respectively. For the ratio to be larger than 1.5 we must have $\omega > 7k^2\nu$. In the $N = 96$ simulations the frequency where the crossover to compressible behavior is observed is $\omega \approx 20k^2\nu$. Below that frequency the results, although somewhat ambiguous, indicate a better agreement between simulations and the correlated theory than with the uncorrelated one.

Nonequilibrium interface roughening

The good accord between theoretical predictions and empirical measurements of the frequency power spectrum can be considered as a validation of the equilibrium properties of ILG interfaces. Figure 7, on the other hand, displays a comparison of simulations of nonequilibrium roughening with predictions from theory. The width W is shown as a function of time for system sizes $N = 16, 32, 64, 96, 128$, and 196; both the width and the time are rescaled in accordance with the prediction of dynamical scaling giving by Eq. (106). The same value of kT_{eff} derived from the frequency power spectra of Fig. 6(a) is also used here to calculate the theoretical curves. The same data are plotted on a log-log scale in Fig. 8.

Four features of the roughening and consequent equilibrium state are notable. First, and most impressive, is the excellent accord, over almost three orders of magnitude, between the predicted $t^{1/3}$ growth of the width and the theoretical prediction. The slight underestimate of the theory may be due to the finite initial width of the interface. Indeed, one can see that for each case the initial values of the width (i.e., the first few time steps) do not match the theoretical growth rate.

The second feature of interest is the sharp crossover from nonequilibrium to equilibrium roughening. The dashed line shows the estimate of the crossover time given in Eq. (113).

The third feature of note is the applicability of the dynamical scaling relation of Eq. (106). However, whereas dynamical scaling holds for all interface sizes during the transient growth, it holds only for $N \leq 64$ for the static interface width. For $N > 64$, the asymptotic width scales as $W \sim (L/\ln L)^{1/2}$ rather than $W \sim L^{1/2}$ as predicted by theory. There are several possible explanations for this breakdown of scaling for large L. First, the logarithmic factor might possibly be due to k-dependent corrections to transport coefficients which are known to exist in two-dimensional hydrodynamics and have been observed in lattice-gas simulations [23,39]. However, since neither viscosity nor diffusivity determines our estimates of asymptotic roughness, this explanation seems inadequate. Another possibility is that the ILG surface tension

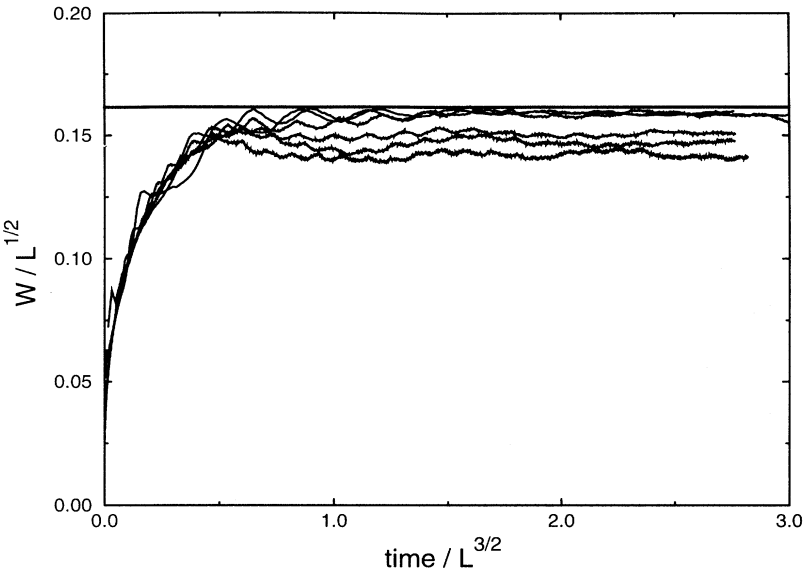

FIG. 7. The root-mean-square interface width W as a function of time for simulations of the immiscible lattice gas. The time t is scaled as $t/L^{3/2}$ and W as $W/L^{1/2}$. The system sizes are $N = 16$, 32, 64, 96, 128, and 196, and the lower values of W/L correspond to larger L. The straight line shows the theoretical predictions in Eq. (104).

may be size dependent, but this has never been noted previously. Lastly, kT_{eff} may itself be size dependent, due to correlations that arise from the time-irreversible ILG collision rules. This last explanation seems the most plausible, but, like each of the effects noted above, it seems unlikely because the logarithmic correction is not observed for $N \leq 64$.

Finally, we note that the scaled asymptotic roughness is seen to be rather small. For example, when $N = 32\sqrt{3}/2$, the asymptotic roughness $W \approx 0.8$ lattice units. Hence the ratio between the wavelength and system size is small, as assumed at the outset of our analysis.

In summary, we find that the predictions of fluctuating incompressible hydrodynamics are clearly evident in the ILG simulations. Thus, despite the fact that the ILG's microdynamics is time irreversible, the concept of an effective temperature that quantifies the coupling between the interface and bulk excitations appears to be meaningful.

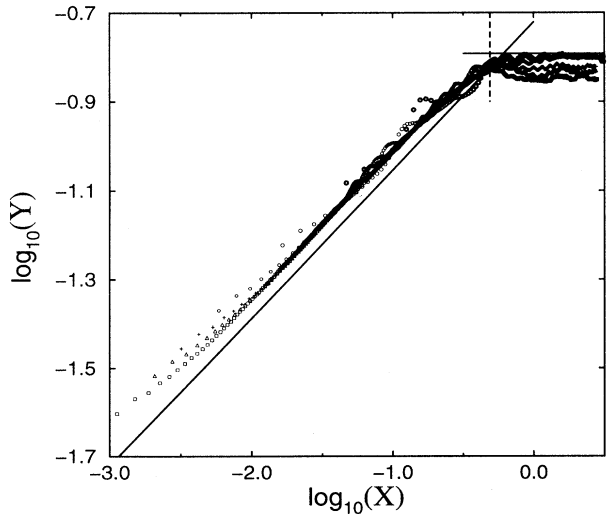

FIG. 8. The same data as in Fig. 7 in a log-log plot with $Y = W/L^{1/2}$ and $X = t/L^{3/2}$. The straight, full lines show the theoretical predictions given in Eqs. (104) and (112), and the dashed line shows the predicted crossover time given in Eq. (113). The system sizes are $L = 16(\circ)$, $32(\circ)$, $64(\circ)$, $96(+)$, $128(\triangle)$, $196(\square)$.

VIII. CONCLUSIONS

We have studied equilibrium and nonequilibrium fluctuating fluid interfaces, both theoretically and by simulation. Our principal theoretical contributions are a fluctuation-dissipation theorem, based on fluctuating incompressible hydrodynamics, and a corresponding equation of motion for a hydrodynamic interface. This equation of motion is written in terms of the interface degrees of freedom only, and it is non-Markovian except in the high viscosity limit. The correlations of the force $\tilde{F}_{\mathbf{k}}$ acting on the interface have been derived explicitly and shown to have a finite correlation time $(k^2\nu)^{-1}$. A complete description of an interface in a thermally excited fluid is obtained when $\tilde{F}_{\mathbf{k}}$ is taken as the driving force in the equation of motion. Comparison between this description and a description which is simplified by neglecting the force correlations has been made. From the fully correlated theory we have derived both the frequency power spectrum that characterizes the equilibrium state of the fluid and the nonequilibrium behavior that results when the interface relaxes from an initially flat state. For two-dimensional fluids, the theory predicts that interfaces roughen in a manner that satisfies a dynamical (or finite-size) scaling law. The key features of the predictions are well confirmed by simulations of fluctuating hydrodynamic interfaces performed with a

momentum-conserving lattice-gas model.

Interestingly, the predicted dynamical scaling properties of fluctuating interfaces in two-dimensional fluids match those of the Kardar-Parisi-Zhang equation [15]. This accord appears to be merely a coincidence, since the KPZ equation describes an entirely different—and purely local—growth dynamics. Nevertheless, our study of fluid interfaces represents a hydrodynamic application of concepts usually applied to simpler local aggregation phenomena.

Our results for dynamical roughening are perhaps most interesting for two-dimensional fluids where the asymptotic interface width has a significant dependence on the system size L. In this case, the time-dependent width $W(t) \sim t^{1/3}$ up to a sharply defined crossover time of the order of the longest capillary wave period of the system. For three-dimensional fluids the roughening at long times is a $\ln t$ growth. Thus it appears that experimental study of roughening fluid interfaces would probably be most revealing in two-dimensional fluids. The two-dimensional hydrodynamics of soap films [40] might possibly offer an opportunity for such experiments.

Lastly we wish to emphasize that our study represents the most detailed validation to date of the dynamics of moving interfaces in lattice-gas automata. Both the $t^{1/3}$ growth of the roughness and the frequency power spectrum of the equilibrium fluctuations result from hydrodynamics coupled to fluctuations. The good accord seen between theory and simulation indicates that the immiscible lattice gas captures the principal features of fluctuating multiphase fluids from mesoscopic to macroscopic scales. In particular, the fluctuation dynamics have been probed and verified over a frequency spectrum ranging from the slow behavior of viscous diffusion to the relatively rapid dynamics of capillary wave oscillations and finally to the high frequency cutoff set by compressibility effects (sound waves). However, to obtain our results we have had to define an effective temperature in the lattice gas. Moreover, there are weak logarithmic corrections to the scaling of the asymptotic width of the largest interfaces. From a theoretical point of view, both of these issues could perhaps be resolved by performing a Green-Kubo analysis of the fluctuating hydrodynamics [41]. Such work, possibly in conjunction with simulations of fluctuating interfaces in three dimensions, is one of the most promising avenues of future theoretical study.

ACKNOWLEDGMENTS

We thank Dik Harris and Knut Jørgen Måløy for valuable discussions. We are also grateful to Howard Stone for his critical and thoughtful remarks and for greatly improving Appendix A. We thank Reuven Zeitak for useful comments and for solving the integral of Eq. (111). This work was supported in part by NSF Grant No. 9218819-EAR and by the sponsors of the MIT Porous Flow Project. E. G. Flekkøy acknowledges support by NFR, the Norwegian Research Council for Science and the Humanities, Grant No. 100339/431.

APPENDIX A: THE GREEN'S IDENTITY

In the following we derive the Green's identity which, together with the correlation function for the force density, forms the basis for the derivation of the fluctuation-dissipation theorem. It is also derived in Ref. [8], although on a slightly different basis. Using Gauss's theorem and the hydrodynamic equations of motion, the following derivation relates the fluctuating force in the bulk to the fluctuating force $\tilde{F}$ on the interface. We assume that the driving force $\mathbf{f}(\mathbf{x},t)$ satisfies $\mathbf{f}(\mathbf{x},t) = \mathbf{0}$ when $|t| > T'$ or when $|z| > l'$. Thus, on account of the dissipative nature of our system, the fluctuating velocity $\tilde{u}$ will vanish outside some distance l from the interface which is sufficiently much larger than l' and outside the time interval $[-T,T]$ where T is sufficiently much larger than T'. In the end we can always take T' and l' to infinity.

The average and fluctuating equations may be written

$$-\rho\frac{\partial\bar{\mathbf{u}}'}{\partial t} = \nabla\cdot\bar{\boldsymbol{\sigma}}, \tag{A1}$$

$$\rho\frac{\partial\tilde{\mathbf{u}}}{\partial t} = \nabla\cdot\tilde{\boldsymbol{\sigma}} + \mathbf{f}. \tag{A2}$$

Here we have used the notation $\bar{\mathbf{u}}' = \mathbf{u}(\mathbf{x},-t)$ to denote time reversal. The time reversed velocity appears also in $\bar{\boldsymbol{\sigma}}$ and it is responsible for the minus sign on the left hand side of Eq. (A1). By taking the inner product of $\bar{\mathbf{u}}'$ with Eq. (A2) and the inner product of $\tilde{\mathbf{u}}$ with Eq. (A1) and subtracting we get

$$\begin{aligned}-\rho\frac{\partial(\bar{\mathbf{u}}'\cdot\tilde{\mathbf{u}})}{\partial t} &= \tilde{\mathbf{u}}\cdot\nabla\cdot\bar{\boldsymbol{\sigma}} - \bar{\mathbf{u}}'\cdot\nabla\cdot\tilde{\boldsymbol{\sigma}} - \bar{\mathbf{u}}'\cdot\mathbf{f}\\ &= \nabla\cdot(\bar{\boldsymbol{\sigma}}\cdot\tilde{\mathbf{u}}) - \nabla\cdot(\tilde{\boldsymbol{\sigma}}\cdot\bar{\mathbf{u}}') - \bar{\mathbf{u}}'\cdot\mathbf{f}\,,\end{aligned} \tag{A3}$$

where we have used that the velocity fields are divergence-free to simplify the right hand side, i.e., we have applied the identity

$$\begin{aligned}\nabla\cdot(\bar{\boldsymbol{\sigma}}\cdot\tilde{\mathbf{u}}) &= (\nabla\cdot\bar{\boldsymbol{\sigma}})\cdot\tilde{\mathbf{u}} + \bar{\boldsymbol{\sigma}} : \nabla\tilde{\mathbf{u}}\\ &= (\nabla\cdot\bar{\boldsymbol{\sigma}})\cdot\tilde{\mathbf{u}} + 2\mu\bar{\mathbf{E}} : \tilde{\mathbf{E}}\end{aligned} \tag{A4}$$

where $\mathbf{E}$ is the usual rate-of-strain tensor, $\mathbf{E} = \frac{1}{2}[\nabla\mathbf{u} + (\nabla\mathbf{u})^T]$.

By integrating Eq. (A3) over the fluid domain, applying the divergence theorem with the unit normal directed outward from V, and integrating over the time interval $(-T,T)$ we arrive at

$$0 = \int_{-T}^{T}\int_{A} d\mathbf{S}\cdot\tilde{\boldsymbol{\sigma}}\cdot\bar{\mathbf{u}}'\,dt + \int_{-T}^{T}\int_{V}\bar{\mathbf{u}}'\cdot\mathbf{f}dV\,dt\,. \tag{A5}$$

Here we have used $\tilde{\mathbf{u}} \equiv \mathbf{0}$ for $\mathbf{x} \in I$, and $\tilde{\mathbf{u}} \to \mathbf{0}$ as $t \to \pm T$. Equation (A5) is the desired result.

APPENDIX B: THE CORRELATION FUNCTION

We here evaluate the correlation function $\langle h_k(t)h_k^*(0)\rangle$, starting from Eqs. (86) and (68).

Figure 4 shows the integration contour used to evaluate the above integral. The horizontal line below the negative real axis maps to the branch cut of the square root. As the C_R part of the contour gives no contribution the integral is given entirely by the poles at $\omega_\pm \equiv \pm\omega_r - i\omega_i$ and the integration around $C_{\rm cut}$.

In order to evaluate the poles we note that the denominator of the right hand side of Eq. (68) can be written

$$\hat{\gamma}_{\mathbf{k}}(\omega) - \frac{\sigma k^2}{i\omega} = \frac{2\rho}{k(1+k/iq\,)}\left(\omega + \sqrt{1+\frac{k}{iq(\omega)}}\;\omega_0\right) \times \left(\omega - \sqrt{1+\frac{k}{iq(\omega)}}\;\omega_0\right), \tag{B1}$$

where $\hat{\gamma}_k(\omega)$ has been written out. It can be demonstrated numerically that, when Eq. (75) holds, the above expression has simple zero points when the second and third terms on the right hand side are zero. These are just the solutions of the capillary wave dispersion relation Eq. (72). Correspondingly, we then obtain

$$\Gamma_k(\omega) = \frac{k}{2\rho}(1+k/iq)\frac{1}{(\omega-\omega_+)(\omega-\omega_-)}\,. \tag{B2}$$

Noting that when $\omega \to \omega_\pm$, $(1+k/iq) \to (\omega_\pm/\omega_0)^2$, the corresponding residues at the poles are then easily evaluated, giving Eq. (88).

We will evaluate the contribution from $C_{\rm cut}$ only in the long-time limit. The substitution

$$\frac{i\omega}{k^2\nu} - 1 \to -iy \pm \delta\,, \tag{B3}$$

where δ is the distance between the cut and the contour, gives the corresponding values for $\bar{q}_\pm = \pm(\sqrt{i})^*\sqrt{y}$. It is then a straightforward algebraic problem to demonstrate that

$$\begin{aligned}\langle h_k(t)h_k(0)\rangle_{\rm cut} &= \frac{\rho\nu^2\,k_BT}{\pi kL}e^{-k^2\nu|t|}\int_0^\infty dy\; e^{ik^2\nu|t|y}A(y)\\ &= \frac{\rho\nu^2\,k_BT}{\pi kL}\frac{e^{-k^2\nu|t|}}{k^2\nu}\frac{\partial}{\partial|t|}\int_0^\infty dy\; e^{ik^2\nu|t|y}\frac{A(y)}{iy},\end{aligned} \tag{B4}$$

where

$$A(y)\begin{cases} = \sqrt{iy}[1+O(\sqrt{y})] & \text{for small } y \\ \propto y^{-7/2} & \text{for large } y. \end{cases} \tag{B5}$$

In the large-$|t|$ limit the rapidly oscillating exponential factor above will leave only the small-y contribution to the integral. Substitution of the small-y form of $A(y)$ in Eq. (B4) gives a convergent integrand due to the time derivative [which does not commute with the integration when the asymptotic form of $A(y)$ is used]. It follows that

$$\langle h_k(t)h_k(0)\rangle_{\rm cut} = \frac{k_BT\rho\nu}{\pi k^3L}\int_0^\infty dy\;\frac{1}{\sqrt{iy}}e^{ik^2\nu|t|y}\,. \tag{B6}$$

The substitution $u = ik^2\nu|t|y$ then gives

$$\begin{aligned}\langle h_k(t)h_k(0)\rangle_{\rm cut} &= \frac{4k_BT\rho\nu^2}{\pi kL\sigma^2}\frac{1}{(k^2\nu|t|)^{3/2}}\int_0^\infty du\;\frac{e^{iu}}{\sqrt{iu}}\\ &= \frac{2k_BT\;\rho\nu^2}{kL\sigma^2}\;\frac{e^{-k^2\nu|t|}}{(k^2\nu|t|)^{3/2}}\\ &\quad\times\left[1+O\big((k^2\nu|t|)^{-1/2}\big)\right]\,,\end{aligned} \tag{B7}$$

which is Eq. (89).

[1] M. A. Bouchiat and J. Meunier, Phys. Rev. Lett. **23**, 752 (1969).
[2] M. A. Bouchiat and J. Meunier, J. Phys. (France) I **32**, 561 (1971).
[3] X. D. Shi, M. Brenner, and S. R. Nagel, Science **265**, 219 (1994).
[4] M. P. Brenner, X. D. Shi, and S. R. Nagel, Phys. Rev. Lett. **73**, 3391 (1994).
[5] W. Kuhn, Kolloid Z. **132**, 84 (1953).
[6] T. Mikami, R. G. Cox, and S. G. Mason, Int. J. Multiphase Flow **2**, 113 (1975).
[7] L. D. Landau and E. M. Lifshitz, *Fluid Mechanics* (Pergamon Press, New York, 1959).
[8] E. H. Hauge and A. Martin-Löf, J. Stat. Phys. **7**, 259 (1973).
[9] B. Alder and T. Wainwright, Phys. Rev. Lett. **18**, 968 (1970).
[10] E. G. Flekkøy and D. H. Rothman, Phys. Rev. Lett. **75**, 260 (1995).
[11] *Dynamics of Fractal Surfaces*, edited by F. Family and T. Vicsek (World Scientific, Singapore, 1991).
[12] J. Krug and H. Spohn, in *Solids far from Equilibrium*, edited by C. Godrèche (Cambridge University Press, Cambridge, England, 1992), pp. 479–582.
[13] P. Meakin, Phys. Rep. **235**, 189 (1993).
[14] S. F. Edwards and D. R. Wilkinson, Proc. R. Soc. London, Ser. A **381**, 17 (1982).
[15] M. Kardar, G. Parisi, and Y. C. Zhang, Phys. Rev. Lett. **58**, 2087 (1987).
[16] F. Family, J. Phys. A **19**, L441 (1986).
[17] F. Family and T. Vicsek, J. Phys. A **18**, L75 (1985).
[18] U. Frisch, B. Hasslacher, and Y. Pomeau, Phys. Rev. Lett. **56**, 1505 (1986).
[19] U. Frisch *et al.*, Complex Syst. **1**, 648 (1987).
[20] D. H. Rothman and J. Keller, J. Stat. Phys. **52**, 1119 (1988).
[21] D. H. Rothman and S. Zaleski, Rev. Mod. Phys. **66**, 1417 (1994).

[22] S. Wolfram, J. Stat. Phys. **45**, 471 (1986).
[23] L. Kadanoff, G. McNamara, and G. Zanetti, Phys. Rev. A **40**, 4527 (1989).
[24] G. Zanetti, Phys. Rev. A **40**, 1539 (1989).
[25] P. Grosfils, J.-P. Boon, R. Brito, and M. Ernst, Phys. Rev. E **48**, 2655 (1993).
[26] A. J. C. Ladd and M. E. Colvin, Phys. Rev. Lett. **60**, 975 (1988).
[27] D. F. M. A. van der Hoef and A. J. C. Ladd, Phys. Rev. Lett. **67**, 3459 (1991).
[28] J. A. Somers and P. C. Rem, Physica D **47**, 39 (1991).
[29] C. Adler, D. d'Humières, and D. Rothman, J. Phys. (France) I **4**, 29 (1994).
[30] E. J. Hinch, J. Fluid Mech. **72**, 499 (1975).
[31] H. K. Moffatt, J. Fluid Mech. **18**, 1 (1964).
[32] C. Pozrikidis, J. Fluid Mech. **202**, 17 (1989).
[33] E. H. Lucassen-Reynders and J. Lucassen, Adv. Colloid Interface Sci., 348 (1969).
[34] J. C. Herpin and J. Meunier, J. Phys. (Paris) **35**, 847 (1974).
[35] S.-K. Ma, *Statistical Mechanics* (World Scientific, Singapore, 1985).
[36] S.-M. Yang, Ph.D. thesis, California Institute of Technology, 1985.
[37] M. Grant and R. C. Desai, Phys. Rev. A **27**, 2577 (1983).
[38] A. J. C. Ladd, J. Fluid Mech. **271**, 285 (1994).
[39] G. R. McNamara, Europhys. Lett. **12**, 329 (1990).
[40] Y. Couder, J. Chomaz, and M. Rabaud, Physica D **37**, 384 (1989).
[41] M. H. Ernst and J. W. Dufty, J. Stat. Phys. **58**, 57 (1990).

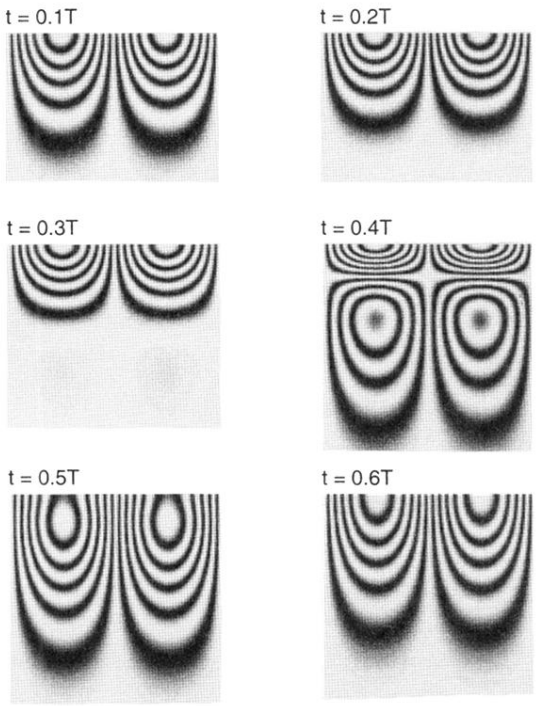

FIG. 3. The streamlines shown at various instants of time t. The thicker streamlines correspond to a smaller velocity. T is the period of the oscillations. The ratio of the viscous time to the period (times 2π) is $\alpha = \omega/(k^2\nu) = 1$. The horizontal base of each figure is one wavelength $2\pi/k$.